Texas A&M University
Mechanical Engineering Department

Measurement of Unbalance Response in a SFD-Rotor Kit - Centered Damper -

by

Dr. Luis San Andres
Associate Professor

Hector Laos
graduate research assistant

Aquiles Lopez
undergraduate student worker

A Research Progress Report
to the
Turbomachinery Research Consortium

May 1994

TRC Project: Experimental and Analytical Study of the Non-Linear Response of Squeeze Film Damper Supported Rotors

Principal Investigators: Drs. S. Noah and L. San Andres

TABLE OF CONTENTS

Introduction

Light weight, high performance jet engines exhibit a trend toward increased flexibility and sensitivity to unbalance, leading to higher than desired vibration levels and reduced reliability. One method to control this sensitivity uses squeeze film dampers (SFDs) to allow journal precessional motions to displace a thin film of lubricant and provide the required mechanism of viscous damping (energy dissipation). Dampers are installed on the outer race of conventional rolling element bearings and can operate with and without an external flexible element. In the first case, a centralizing spring aids the damper to support a static load, typically a fraction of the rotor weight; while on the second, the damper itself needs to provide hydrodynamic forces to assure lift-off without solid contact. To date experience has shown that squeeze film damper performance ranges from good to erratic, and sometimes non-functioning despite analytical predictions to the contrary.

The TAMU rotordynamics laboratory has a vast experience on the experimental measurement of forces in squeeze film dampers and development of analytical models for damper dynamic force prediction. The dynamic performance of SFDs is largely affected by a number of design and operating parameters. In general, the combination of a soft centering stiffness and high viscous damping will prove successful to reduce vibration amplitudes at critical speeds and moderate levels of unbalance conditions. Large lubricant pressure supply will tend to improve the operation by preventing liquid cavitation and the appearance of cross-coupled damping forces. On the other hand, excessive levels of unbalance can lead (in theory) to multiple valued responses with damper lock-up at system resonances, and even aperiodic and chaotic response in certain narrow speed ranges. In addition, operation at large speeds in dampers with increased clearances can be affected by fluid inertia forces, and worse yet, by lubricant material decomposition into an emulsion (mixture of liquid and vapor) unable to sustain the large system motions and deliver the required levels of damping forces needed for safe operation.

In theory, dampers are regarded as highly non-linear systems which provide forces depending on the instantaneous values of journal velocity and complex functional forms of the eccentricity. Current theoretical dynamic analyses of rotor-disk assemblies supported on SFDs are based on overly simplified analytical expressions for damper fluid film forces as derived from the short journal bearing model with the so-called π film cavitation assumption. Computational predictions based on step-by-step numerical predictions, and lately analytical results based on current non-linear dynamics models with elegant mathematical methods, have shown that the forced response of rotor-SFDs systems is highly non-linear with extreme sensitivity to unbalance levels. Little effort has been placed on finding a combination of operating and design damper parameters which will avoid this undesirable response. On the other hand, the "richness" of the non-linear behavior has been exploited to extend beyond limits the amazing accuracy of the non-linear models. At this time it is worth to mention that there is little physical evidence and practical experience which attest to the veracity of the theoretical predictions. In fact, in the last three years, over 20 theoretical technical manuscripts have appeared on the literature and not a single one has investigated the phenomenon by experimental means, or even worse has provided a sound set of conditions (of practical value) for the

development of an experiment directed to validate (or disprove) the theoretical findings. The profusion of recent theoretical results addressing to the non-linear aspects of rotors mounted on SFDs, has motivated the design and construction of a small test apparatus for the measurement of the dynamic forced response of a rigid rotor supported on open-ends SFDs with centering springs. The experimental set-up has been kept simple enough to provide a means for correlation with analytical predictions but at the same time considering the important aspects of a practical application.

This research progress report presents a description of the SFD test apparatus and the measurements performed to identify the effects of squeeze film damper forces on the dynamic response of a rotating structural system. The test rig mechanical components are presented along with a description of the squeeze film damper element. The test procedure and instrumentation for collection of dynamic motion data for coast-down tests at a controlled rotor deceleration rate are presented. Experimental results for the natural frequencies of the system are shown along with calculated predictions obtained using a commercial rotordynamics code. Measurements of the dynamic force response with different disk unbalance levels are presented and discussed in detail. A simple analytical model describing the dynamics of the rotor-SFD system at rotational speeds below the first elastic critical speed is also presented.

Description of rotor-SFD test apparatus

Figure 1 shows a photograph of the test apparatus and instrumentation used on the investigation. Figure 2 depicts a cross-sectional view of the rotor and squeeze film damper along with the notation used to identify the system major components. The test apparatus consists of a steel shaft supported at two locations and with an overhung disk attached at one of the shaft ends. The configuration resembles that of a cantilever (overhung) rotor and effectively simulates a geometrical arrangement found in the aft compressor section in aircraft engines. The rotating system is connected with a flexible coupling to a variable speed DC motor with a top speed of 10,000 rpm and nominal power equal to 1/10 HP. At the driving motor end, the steel shaft of diameter 1/8 in. is supported with a brass bearing bushing backed with an elastomeric element (O'ring). Static measurements prior to system assembly showed that the stiffness of this support is equal to 850 lb/in.

The squeeze film damper and shaft support squirrel cage structure are shown in Figure 3. Four soft steel rods are connected on of their sides to a base structure, while the other sides are attached to a cylindrical steel body also working as the journal of the squeeze film damper. The shaft is press fitted on two ball bearings which are inserted with a tight fit on the interior surface of the journal. The weight of the journal and ball bearings is equal to 1.79 lbs. Static force versus deflection measurements of the squirrel cage determined values of structural stiffnesses equal to 850 lb/in and 820 lb/in in the vertical and horizontal directions, respectively.

The squeeze film damper element consists of a plexiglass housing connected rigidly to a steel support. The inner surface of the housing fits loosely into the outer surface of the journal connected to the squirrel cage. The damper nominal length (**l**) and diameter (**D**) are equal to 1.0 and 2.0 inches, respectively. The radial film clearance (**C**) is equal to 0.010 inches with a

variation for out-of-roundness of +/- 0.0015 inches. The squeeze film damper has both ends open to ambient conditions, and its geometric **L/D** and **D/C** ratios are equal to 0.50 and 200, respectively. Lubricant is fed at the damper housing midplane top section with a capillary tube providing a high flow resistance to avoid back-flow through the fluid supply lines. A small gear pump (maximum flow 0.32 GPM and 12 psig) is used to deliver the lubricant to the damper, and a thermocouple and pressure gauge are installed just upstream of the capillary flow inlet. The lubricant used on the experiments corresponds to a Mobil No.3 oil with a specific gravity equal to 0.81 and viscosity values of 0.0028 Pa-sec and 0.001784 Pa-sec at 68°F and 104°F (20° to 40°C), respectively. Most experiments were carried out at an inlet oil temperature equal to 85.1°F (29.5°C) with a corresponding viscosity equal to 0.00225 Pa-sec.

The end disk with a weight of 1.79 lbs, and a diameter and width equal to 3 and 1 inches, respectively, has a series of machined holes spaced 22.5° apart at a radius equal to 1.2 inches. Calibrated weights can be inserted on these holes to provide a controlled unbalance force to excite dynamically the rotor-damper system. Pairs of non-contacting displacement sensors of the eddy-current type are located at different positions on the test rig. The sensors are orthogonally positioned (vertical-Y and horizontal-X directions) at designated locations 1 through 4 as shown in Figure 4. Location 1 is closest to the end disk while location 4 is just next to the brass bushing and O'ring support. Locations 2 and 3 are on the sides of the squeeze film damper element. Two additional displacement sensors are positioned next to the driving motor, one to provide a key-phasor signal and the other one for feedback control of the driving DC motor speed.

Figure 5 shows a schematic view of the major pieces of instrumentation used on the investigation. An eight-channel analog signal conditioner, one digital vector filter, one spectrum analyzer and two oscilloscopes are used to measure the dynamic forced response of the rotor-damper system as the rotor speed decreases with a constant deceleration rate for different levels of unbalance masses at the end disk. The lubricant inlet temperature and pressure to the SFD are also kept constant, and visual observations of the flow field within the damper film lands are possible since the damper housing is transparent. Orbital shaft motions at locations 1 and 3 are displayed continuously on the oscilloscopes, and the spectrum analyzer shows the frequency content of the shaft vertical motion at locations 1 and 3. The digital vector filter is connected directly to an HP-9000 series computer via a HP-IB interface. The ADRE rotordynamics software is used to measure and analyze the dynamic forced response of the rotor at one shaft location (X-Y rotor displacements typically at location 1), to calculate frequency spectrum cascade plots, as well as to direct storage and access of the acquired data from the test apparatus for further manipulation.

It is important to note here that the rotor-damper system described here corresponds to the third configuration tried. The first two configurations used a longer shaft providing more system flexibility, a rigid ball bearing support on the drive motor end, and with an unbalance disk between the ball bearing support and the squirrel cage support located at the other shaft end. Computed predictions from an undamped rotordynamics model showed large amplitude motions at the location of the squirrel cage support for the first mode of vibration (rigid body

conical) . Once the system was assembled, early dry-tests (without oil in the damper) verified the predictions. However, when oil flowed through the damper, the first mode of vibration completely disappeared due to the large amount of damping available and the flexibility of the shaft used. On the other hand, the second mode (first flexural mode) showed large amplitude vibrations with the damper located right at a nodal point. These unexpected results delayed considerably the experimental effort and confirmed the very limited use of an undamped rotordynamics model.

Experimental results

Calibrated shims were required to align all the system elements. The damper housing was centered relative to the journal surface using dial gauges in the vertical and horizontal directions along with a complicated method which included direct measurements of the damper maximum and minimum clearances and careful repositioning of the damper housing. This tedious procedure determined finally the journal to be centered within the damper housing with a confidence of 0.001 and 0.0005 inches in the vertical and horizontal directions, respectively. The rotor was carefully balanced under dry conditions (no lubricant in the damper) using the influence coefficient method applied to an overhung rotor (Worth, 1981). A final trim balancing brought a maximum peak to peak orbital motion of less than 0.001 inches at position 1, next to the balancing disk for rotor speeds to 5,000 rpm.

Free response measurements at zero rotational speed

The rotor was excited with a calibrated impact hammer at the disk location and the free vibration response without shaft rotation was measured at position 1 (next to the unbalance disk). Figures 6 and 7 show the free decay response for the system without oil (dry condition) and with lubricant flowing through the squeeze film damper. The dry tests show a natural frequency equal to 34.1 Hz, and a logarithmic decrement equal to 0.0622 corresponding to an equivalent damping ratio at location 1 equal to $\xi=0.010$. The free decay measurements for the system with oil were taken at a fluid temperature equal to 20°C ($\mu=0.0028$ Pa.sec). The results show a natural frequency equal to 32.25 Hz with a logarithmic decrement of 0.779 corresponding to a damping ratio equal to $\xi=0.121$. Note that the simple addition of lubricant in the damper raised the overall damping in the system by an order of magnitude. The damping ratios measured correspond to equivalent damping coefficients at location 1 approximately equal to 0.020 and 0.24 lb.sec/in for the dry and lubricated damper conditions, respectively.

Similar results were obtained from the force/displacement transfer function curves displayed on the frequency analyzer. Additional measurements were also taken at location 3. These measurements show the shaft motion at this position to be in phase with that of location 1. Furthermore, the displacement measurements at the four locations along the shaft axis demonstrate that the fundamental mode of free vibration was very close to conical. Further details on this topic will be given later as a justification for the analytical model used.

Measurements of the system forced response to rotor unbalance

Experimental measurements of the system dynamic forced response were performed for

increasing levels of disk unbalance as the rotor coasted down from a top speed of 5,000 rpm and at a constant deceleration rate approximately equal to 3,800 rpm/min. The lubricant to the damper was kept at a level of pressurization equal to 5 psi above ambient and at an inlet temperature of approximately 85°F (29.5°C) with a fluid viscosity of 0.00225 Pa.sec. Figures 8 and 9 show the vertical and horizontal rotor forced response measured at location 1 for unbalance masses corresponding to 1.0, 2.0 and 2.7 grams inserted on the disk at a radial distance equal to 1.2 inches. The curve labeled 0 grams corresponds to the base line trim balanced rotor response. The response curves presented show peak-to-peak amplitudes without any synchronous filtering. Note that the experimental results correspond to a SFD centered within the bearing housing. Figure 10 shows a frequency cascade plot of the vertical rotor response as the system speed decreases for a disk unbalance mass equal to 2.7 grams. The results show no trace of **asynchronous** frequency components in the unbalance forced response at location 1. The measurements show that at the critical speed the vertical amplitude of motion is about 1.25 times the horizontal response, and consequently, the shaft orbits at location 1 are elliptical as a consequence of the stiffness asymmetry on the squirrel cage supports (figures showing shaft orbits at locations 1 and 3 are given later). Note also that the location of maximum amplitude vibration and which defines the system first critical speed shifts (slightly) towards higher speeds as the disk unbalance level increases. This observation appears to confirm that the squeeze film damper provides a radial stiffness as the SFD operating dynamic journal eccentricity increases.

Figures 11 and 12 show the rotor vertical and horizontal dynamic response at location 3 for the same conditions of disk unbalance detailed above. The ratio of vertical to horizontal peak-to-peak amplitudes is also approximately equal to 1.25. Figure 13 depicts a cascade frequency plot of the vertical response as the rotor speed decreases for the largest level of disk unbalance. The measurements show the frequency spectra lines to be mostly composed of synchronous frequency components. At the largest rotor speeds, the vibration amplitudes start to increase since the rotor-damper system is approaching its second critical speed (approximately at 6,960 rpm) and which corresponds to the first system flexural mode.

Figures 14 and 15 show shaft orbits at locations 1 and 3 at rotor speeds equal to 2,057 rpm and 5,065 rpm, respectively, and for a disk unbalance equal to 2.7 grams. The largest magnitudes of vibration were measured at the system first critical speed at 2057 rpm (34.3 Hz). At this speed, the vibration signals at locations 1 and 3 are closely in phase as evidenced by the keyphasor marks on the orbits displayed on Figure 14. On the other hand, at the largest speed tested (5,065 rpm), the vibration amplitudes at locations 1 and 3 are similar in magnitude, form circular orbits at both positions, but also show an evident phase shift increasing to 90° (in relationship to keyphasor marks) between the two vibration signals at shaft locations 1 and 3. The measurements at the highest speed demonstrated that the SFD was not very effective in controlling shaft excursions for rotor speeds around the system second critical speed.

For this centered squeeze film damper configuration, non-synchronous motions were not ever observed or measured even at different rotor deceleration rates. The results also demonstrate a shift of the first critical speed to higher rotational speeds as the disk unbalance

level increased denoting (perhaps) the existence of a radial stiffness from the squeeze film action. Thus, the observed system forced response due to the levels of disk unbalance used is eminently linear. It is important to note that visual observations of the lubricant flow within the damper film lands were very useful to elucidate some important aspects of the damper forced response. For the lowest levels of unbalance, 1 and 2 grams, and as the system passed through the critical speed (approx. 2,000 rpm), some lubricant "striations" appeared to rotate around the damper journal at very low frequencies and some lubricant fine bubbling developed within the damper film lands. On the other hand, for the largest level of unbalance (2.7 grams), the lubricant within the damper film lands was observed to have a non-uniform behavior, generating a "burping" sound as if oil bubbles were collapsing under the dynamic action of the journal motion. The lubricant did not fill the entire film lands and the phenomena appeared to be chaotic in nature. The behavior was so unusual as if the fluid (as a continuum) was broken into many pieces which were then expelled from the damper. The phenomena although very complex in nature appeared to be local to the squeeze film damper since the frequency content of the vibration signals at positions 1 and 3 did show only one frequency component, namely the first critical speed. An increase in the damper inlet pressure supply (to 20 psig) did not seem to alleviate the phenomena (i.e., reduce the vibration amplitude), but the lubricant was expelled at a faster rate through the damper discharge sides. Most importantly, an increase in the damper pressurization did not show any effect on the measured amplitude of vibrations or a decrease in the shaft orbits being traced on the oscilloscopes. At present, it is very difficult to describe with any further detail the phenomena observed and in the near future pressure sensors will be installed on the damper housing.

Further tests with larger disk unbalance masses were not performed to protect the test apparatus from excessive amplitude vibrations at the location 1 and at the squeeze film damper. With the largest level of unbalance used, the noise and shaking of the damper housing and base support were so large that further tests would have been disastrous. Later it will be shown that estimated amplitudes of motion at the damper housing reached values very near the damper clearance. On one occasion excessive rotor vibrations may have caused the damper journal to become loose relative to the squirrel cage support. Before realizing this condition, further measurements were taken, and it was then discovered that at rotor speeds about twice the first critical speed (2,000 rpm) a subsynchronous motion appeared at the natural frequency. The amplitude of the subsynchronous vibration component was very large. Some measurements were recorded but not presented or discussed at this time until further information is collected. The subsynchronous motion may have been due to the loose journal or this becoming off-centered relative to the bearing housing. Once the journal was fastened to the squirrel cage disk and the centering procedure reworked, the rotor-damper rig was brought up to 5,000 rpm but no subsynchronous vibrations appeared again.

Modeling of the rotor-SFD test apparatus

A commercial rotordynamics computer code was used to predict the natural frequencies of the rotor-SFD test apparatus. This computational program is based on the transfer matrix method (Myklestad, 1944, Prohl, 1945), and determines the eigenvalues (critical speeds) and damped mode shapes of linear rotor-bearing systems (Vance et al., 1984). For the analysis, the

rotor shaft was divided into 10 stations with stiffness coefficients equal to 850 lb/in at the two bearing support locations. The predicted (undamped) first two natural frequencies for the rotor-damper system are equal to 34.4 and 124.7 Hz, respectively. The calculated first natural frequency correlates well with the measured value of 34 Hz; while the predicted second natural frequency is higher than the one determined experimentally at 116 Hz. Figures 16 and 17 show the calculated mode shapes for the first and second undamped natural frequencies, respectively. Note that the first mode of vibration is close to conical with the shaft acting as a rigid element. On the other hand, the second mode corresponds to the first bending mode of the shaft and shows the damper to be positioned close to a nodal point. The analysis also showed the disk gyroscopic effects to be minimal on the first natural frequency and mode shape of the rotor-SFD test rig.

Figure 18 shows the experimental (vertical and horizontal) vibration shapes of the rotor-SFD test rig as determined from measurements of shaft amplitudes at four axial locations. The measurements were taken at increasing speeds from 1,000 to 5,000 rpm and the figures show normalized magnitude values relative to the maximum displacements measured at each speed. Location 1 is next to the end disk, location 2 corresponds to the damper bearing support, location 3 is in between the damper journal and squirrel cage support, and location 4 is close to the ball bearing support next to the drive motor end. A schematic view of these locations with dimensions is given in Figure 4. The magnitude and keyphasor phase angle of the vibration vectors for the vibration shapes depicted in Figure 18 are given in Table 1. The measurements show that below 4,000 rpm the system has a vibrational shape similar to that of a conical rigid body mode as predicted by the rotordynamics analysis. Note that there is some amount of shaft bending but this appears to be minimal in comparison to the deflection at the squirrel cage (except for the vertical motion at the critical speed). Thus, the first mode shape of the system is largely due to the elastic centering element (squirrel cage).

Based on the experimental measurements, an equivalent mechanical lumped-parameter dynamic model should be accurate enough to predict the rotor response for speeds below 5,000 rpm. The system fundamental mode of vibration can be modeled by simple differential equations of motion at some appropriate axial location in the system. This model is valid if gyroscopic effects are minimal on the dynamic forced response of the rotating system. Fortunately, this is the case for the SFD test apparatus at rotor speeds well below the second natural frequency.

Figure 19 shows the assumed conical modal vibration of the test apparatus and the equivalent lumped parameter model at location Y1. In a conical vibration model, the amplitudes of motion at any material point in the rotor is proportional to a reference point here taken as the motion at shaft location 1. Let Y(z) denote the vertical displacement along the shaft axis, then using simple geometrical relationships, the displacements at the disk (D), squirrel cage (SC), midplane of damper (SFD), and at location 3 are related to the displacement at location 1 (free shaft end) by the following relationships:

Table 1

Synchronous vibration Amplitude (mils peak to peak) and phase angle* at four locations on rotor.
Total amplitude in (), Disk unbalance mass= 2 gr, Temp= 26.6°

Vertical direction

speed (rpm)	P1	P2	P3	P4
1000	3.0 @162° (3.5)	1.7 @125° (2.1)	0.4 @69° (0.6)	0.1 @ - (0.4)
2000	24.7@223° (25.0)	15.6@217° (16.0)	4.3 @242° (4.3)	0.8 @12° (1.0)
3000	9.1 @272° (9.2)	6.3 @276° (6.4)	2.9 @314° (3.0)	0.6 @10° (0.9)
4000	6.4 @262° (6.5)	5.0 @280° (5.0)	3.4 @323° (3.5)	1.2 @ 3° (1.3)
5000	5.9 @243° (5.9)	4.7 @285° (4.7)	5.0 @335° (5.1)	2.6 @ 6° (2.7)

Horizontal direction

speed (rpm)	P1	P2	P3	P4
1000	2.5 @76° (2.9)	1.3 @55° (1.6)	0.7 @42° (1.0)	0.1 @ - (0.4)
2000	18.7@115° (18.2)	13.0@122° (13.4)	5.0 @123° (5.4)	0.1 @ - (0.4)
3000	7.8 @179° (8.1)	6.2 @193° (6.4)	2.9 @206° (3.0)	0.4 @255° (0.5)
4000	5.4 @174° (5.7)	4.8 @201° (4.9)	3.1 @221° (3.3)	0.8 @257° (0.9)
5000	4.3 @165° (4.5)	4.7 @205° (4.8)	4.5 @227° (4.6)	1.7 @253° (1.8)

* Phase angle relative to keyphasor located at horizontal position

$$Y_D = Y_1 Z_D/Z_1 = Y_1 (9.375/10.75)[\text{in/in}] = 0.87\ Y_1$$

$$Y_{SFD} = Y_1 Z_{SFD}/Z_1 = Y_1 (6.00/10.75)[\text{in/in}] = 0.56\ Y_1 \quad (1)$$

$$Y_{SC} = Y_1 Z_{SC}/Z_1 = Y_1 (5.375/10.75)[\text{in/in}] = 0.50\ Y_1$$

$$Y_3 = Y_1 Z_3/Z_1 = Y_1 (3.75/10.75)\ [\text{in/in}] = 0.35\ Y_1$$

The rotor-SFD test rig concentrated (point) masses at the disk and SFD locations are equal to M_D = 1.79 lb (0.8136 kg), and M_{SFD} = 1.79 lb (0.8136 kg), respectively. This last value has been estimated from the damper geometry and not actually measured. The mass of the steel shaft (M_{Sh}) is equal to 0.344 lb (0.1563 kg), based on a material density ρ = 0.283 lb/in^3, with a shaft diameter of 0.375 inches and a length of 11 inches, respectively. The measured stiffness of the squirrel cage (K_{SC}) is K_{SC} = 850 lb/in (149,122 N/m) in the vertical direction.

Equivalent mass and stiffness coefficients at location 1 are easily determined from the total strain and kinetic energy of the system and equal to:

$$M_1 = (M_D Z_D^2 + M_{SFD} Z_{SFD}^2 + 1/3\ M_{sh} Z_{sh}^2)/L_1^2 = 2.13\ \text{lbs}\ (0.968\ \text{kg}) \quad (2)$$

$$K_1 = K_{SC} (Z_{SC}/Z_1)^2 = 212.5\ \text{lb/in}\ (37{,}280\ \text{N/m})$$

The undamped natural frequency for the conical mode is then calculated to be:

$$\omega_{n1} = \sqrt{K_1/M_1} = 196.21\ \text{rad/sec}\ \ (31.22\ \text{Hz}) \quad (3)$$

This value differs by 8% with the measured undamped first natural frequency of 34 Hz. Note that the value predicted neglects any contribution of the O'ring brass bushing support to the system stiffness. Furthermore, the value of the mass for the damper journal and ball bearings is only an estimated magnitude based on the damper geometry. In the analysis that follows, the equivalent mass M_1 has been modified to as to match the measured undamped natural frequency equal to 34 Hz. This modified value M_1 = 1.80 lbs (0.82 kg) can be regarded as a modal mass for the conical mode shape of vibration.

The equations of motion of the rotor-SFD apparatus for rotational speeds well below the first elastic mode (6,280 rpm) are given for displacements in the vertical (Y) and horizontal (X) directions at shaft location 1 as:

$$\begin{aligned} M_1 \ddot{Y}_1 + C_1 \dot{Y}_1 + K_1 Y_1 &= F_{unb.Y1} + F_{SFD.Y1} \\ M_1 \ddot{X}_1 + C_1 \dot{X}_1 + K_1 X_1 &= F_{unb.X1} + F_{SFD.X1} \end{aligned} \quad (4)$$

where C_1 is a viscous damping coefficient not related to the squeeze film damper, $F_{unb,1}$ correspond to the disk unbalance forces and $F_{SFD,1}$ denote the equivalent squeeze film damper

forces at location 1. Note that equations (4) assume any static load to be taken at the equilibrium position by the deflection of the squirrel cage support. Thus, the X and Y coordinates refer to dynamic motions about this static equilibrium position.

The critical damping coefficient for the system described by equations (4) is given by the relationship

$$C_{cr,1} = 2 * \sqrt{K_1 M_1} = 349.70 \text{ Ns/m } (2.00 \text{ lb.sec/in}) \tag{5}$$

The equivalent unbalance and SFD forces at location 1 are determined from the work performed at their locations of action. For constant rotor angular velocity (Ω), the equivalent disk unbalance force components (at 1) are:

$$F_{unb.X1} = m\, r_u\, \Omega^2\, [Z_D/Z_1] \cos(\Omega t)$$

$$F_{unb.Y1} = m\, r_u\, \Omega^2\, [Z_D/Z_1] \sin(\Omega t) \qquad Z_D/Z_1 = 0.87 \tag{6}$$

where m is the disk mass unbalance in $lb.s^2/in$ (kg) inserted at the radial distance $r_u = 1.2$ in (3.048 cm). In most analyses, the unbalance force is expressed in terms of the system equivalent mass, i.e.

$$F_{unb,X} = M_1\, u_1\, \Omega^2 \cos(\Omega t) \tag{7}$$

where u_1 corresponds to the system unbalance displacement. From (6) and (7) it can be easily inferred that

$$u_1 = (m/M_1)\, r_u\, [Z_D/Z_1] \tag{8}$$

The equations of motion for the rotor-SFD system with reference to shaft location 1 are then given as:

$$M_1 \ddot{X}_1 + C_1 \dot{X}_1 + K_1 X_1 = M_1\, u_1\, \Omega^2 \cos(\Omega t) + F_{SFD.X}[Z_{SFD}/Z_1]$$

$$M_1 \ddot{Y}_1 + C_1 \dot{Y}_1 + K_1 Y_1 = M_1\, u_1\, \Omega^2 \sin(\Omega t) + F_{SFD.Y}[Z_{SFD}/Z_1] \tag{9}$$

where $F_{SFD.X}$ and $F_{SFD.Y}$ are the squeeze film damper forces at their place of action, and $Z_{SFD}/Z_1 = 0.56$

For the largest unbalance mass used in the experimental measurements, m=2.7 grams, the calculated value of the unbalance parameter is equal to u = 0.00344 inches (87.4 μm). It is important to note that the experimental measurements at location 1 (see Figures 8 and 9) show a peak-to-peak vertical amplitude of motion equal to 0.0075 inches at the largest rotor speed. This value will then correspond to an unbalance displacement (u) equal to 0.00375 in and very similar to the predicted value. Calculations performed for the other unbalance masses show the

same correlation with the experimental measurements.

The squeeze film damper used in the investigation has a length to diameter ratio (**l/D**) equal to 0.50. Thus, to use the short length, open-ends SFD theory to model the damper fluid film forces is only approximate. These forces are given by (Childs, 1993):

$$F_{SFD.X} = -\mu\, R\, l^3/C^2 \;\; [\![\dot{X}_{SFD}\, I_{11}(\varepsilon) + \dot{Y}_{SFD}\, I_{12}(\varepsilon)]\!]$$

$$F_{SFD.Y} = -\mu\, R\, l^3/C^2 * [\![\dot{X}_{SFD}\, I_{21}(\varepsilon) + \dot{Y}_{SFD}\, I_{22}(\varepsilon)]\!] \qquad (10)$$

The SFD forces are functions of the fluid viscosity, damper geometry and film clearance, journal center velocities, and the following bearing integral functions which depend on the instantaneous film thickness:

$$I_{ij}(\varepsilon) = \int_{\theta} \sin^i(\theta) * \cos^j(\theta)/[1+\varepsilon\cos(\theta)]^3 \, d\theta \qquad (11)$$

and $$\varepsilon = e/C = \sqrt{(X_{SFD}^2 + Y_{SFD}^2)}/C \qquad (12)$$

is the dynamic journal center dimensionless displacement (eccentricity). The SFD model used to arrive to the force expressions given by equation (10) regards the fluid as isoviscous and incompressible, and furthermore, it assumes the flow to be laminar and inertialess. A simple calculation shows that the squeeze film Reynolds number ($\rho\omega c^2/\mu$) at a whirl frequency coinciding with the natural frequency (ω_n=213.6 rad/s [34 Hz]) is equal to 4.82 at an oil operating temperature of 29.5° C. This Reynolds number denotes a damper configuration where fluid inertia effects may be of importance. (Note that an estimated added fluid mass of 0.344 kg is found from the well known formulae $M_{inertia}=\pi\rho RL^3/12C$).

The equivalent equations of motion for the system at location 1 are finally written as:

$$\begin{aligned} M_1 \ddot{X}_1 + C_1 \dot{X}_1 + K_1 X_1 &= M_1 u_1 \Omega^2 \cos(\Omega t) - \mu\, R\, l^3/C^2\, (Z_{SFD}/Z_1)^2\, [\![\dot{X}_1\, I_{11}(\varepsilon) + \dot{Y}_1\, I_{12}(\varepsilon)]\!] \\ M_1 \ddot{Y}_1 + C_1 \dot{Y}_1 + K_1 Y_1 &= M_1 u_1 \Omega^2 \sin(\Omega t) - \mu\, R\, l^3/C^2\, (Z_{SFD}/Z_1)^2\, [\![\dot{X}_1\, I_{21}(\varepsilon) + \dot{Y}_1\, I_{22}(\varepsilon)]\!] \end{aligned} \qquad (13)$$

where $I_{ij}(\varepsilon)$ depend on $X_{SFD} = X_1 Z_{SFD}/Z_1$ and $Y_{SFD} = Y_{1Z} Z_{SFD}/Z_1$

Conversely, these same equations of motion could be expressed with reference to the displacement coordinates at the damper location, i.e.

$$M_{SFD} \ddot{X}_{SFD} + C_{SFD} \dot{X}_{SFD} + K_{SFD} X_{SFD} = M_{SFD} u_{SFD} \Omega^2 \cos(\Omega t)$$

$$-\mu\, R\, l^3/C^2 \;\; [\![\ddot{X}_{SFD}\, I_{11}(\varepsilon) + \ddot{Y}_{SFD}\, I_{12}(\varepsilon)]\!]$$

$$M_{SFD}\, \ddot{Y}_{SFD} + C_{SFD}\, \dot{Y}_{SFD} + K_{SFD}\, Y_{SFD} = M_{SFD} u_{SFD}\, \Omega^2 \sin(\Omega t) \qquad (14)$$
$$-\mu\, R\, l^3/C^2 \;\; [\![\dot{X}_{SFD}\, I_{21}(\varepsilon) + \ddot{Y}_{SFD}\, I_{22}(\varepsilon)]\!]$$

where
$M_{SFD}=M_1(Z_1/Z_{SFD})^2 = 2.615$ kg (5.75 lb),
$K_{SFD}=K_1(Z_1/Z_{SFD})^2 = 118{,}877$ N/m (679.3 lb/in), and
$C_{cr,SFD}=C_{cr,1}(Z_1/Z_{SFD})^2 = 1{,}116$ Ns/m (6.37 lb.sec/in) (15)

are the equivalent system parameters at the SFD location, and
$u_{SFD} = (m/M_{SFD})r_u[Z_D/Z_{SFD}] = u_1\, [\, L_{SFD}/L_1]$
is the equivalent unbalance parameter. It is common in the theoretical analysis of rigid rotors mounted on SFDs to define a bearing parameter (B) as

$$B = \mu\, R[l^3/C^3]/\, M_{SFD}\omega_1 \qquad (16)$$

For a fluid viscosity equal to 0.00225 Pa.s at 29.5° C, this bearing parameter is equal to 0.1023 for a system natural frequency of 213.6 rad/sec (34 Hz). The value of B corresponds to a very lightly damped system and quite representative of an actual application (ξ=B according to Vance, 1988).

Estimated experimental values for the SFD linear damping coefficients

For a **linear** isotropic rotor-bearing system, the amplitude of vibration at resonant conditions, i.e. forced excitation at the system natural frequency, is equal to:

$$A_{crit.1}/u_1 = 1/2\xi \qquad (17)$$

where $\xi = C_{*1}/C_{cr.1}$, and $C_{cr.1}$=349.7 Ns/m (2.00 lb.sec/in) for the test apparatus. From the maximum response to unbalance measured at shaft location 1 and depicted in Figures 8 and 9, the damping ratio can be evaluated. An estimate for the experimental damping coefficient at the SFD can be determined from the following relationship:

$$C_{SFD} = [C_{*1}-C_{dry}]\, [\![Z_1/Z_{SFD}]\!]^2 \qquad (18)$$

where Z_1/Z_{SFD}=1.786, and C_{dry}=0.020 lb.sec/in (3.50 N.s/m] is the system damping determined from the free vibration measurements without fluid in the damper. Table 2 provides a summary of the estimated values for the system and SFD **linear** damping coefficients as extracted directly from the measurements.

TABLE 2 - Estimated experimental damping coefficients from amplitude measurements at the system critical speed.

m_u (grams)	A_{crit} (mils)	u_1 (mils)	A_{crit}/u	ξ	C_{*1} lb.sec/in	C_{SFD} lb.sec/in
2.7	19.5 16.0	3.45	5.65 4.63	0.088 0.108	0.176 0.216	0.500 0.690
2.0	13.0 11.5	2.55	5.10 4.50	0.098 0.110	0.196 0.222	0.565 0.643
1.0	7.0 5.5	1.28	5.48 4.29	0.091 0.116	0.182 0.233	0.517 0.678

first row: vertical (Y) displacement, second row: horizontal (X) displacement

From the system free vibration response curve shown in Figure 7 and with oil on the damper, a system damping coefficient C_{*1} equal to 0.24 lb.sec/in was determined. This value corresponds to a squeeze film damping coefficient C_{SFD} equal to 0.76 lb.sec/in. Note that the free decay results were taken with oil at a lower temperature (20°C) than for the dynamic forced response tests. The extracted experimental results for the SFD damping coefficient appear to be consistent.

Analytical values for the squeeze film damper coefficients

For circular centered motions, the direct (C_{tt}) and cross-coupled (C_{rt}) damping coefficients are defined by the following expressions based on the π film cavitated solution for the short length, open ends SFD model (Vance, 1988):

$$C_{tt} = \pi \mu R (l/C)^3 / [\![2(1-\varepsilon^2)^{3/2}]\!]$$

$$C_{rt} = 2 \mu R (l/C)^3 \varepsilon /(1-\varepsilon^2)^2 = K_{rr} /\Omega \qquad (19)$$

where $\epsilon = e/C$ is the dimensionless orbit radius or journal eccentricity and K_{rr} is the frequency dependant radial stiffness of the SFD.

The disk unbalance masses equal to 1, 2 and 2.7 grams correspond to dimensionless unbalance parameters u_{SFD}/C equal to 0.071, 0.142, and 0.192, respectively. For these same levels of unbalance and the system critical speed, the maximum amplitudes of motion at the damper location are estimated to be equal to 3.52, 6.85 and 9.92 mils. These values are based on an arithmetic average of the measured vertical and horizontal amplitudes at rotor location 1. The amplitudes of motion at the damper correspond to dimensionless orbit radius (ϵ) equal to 0.35, 0.68 and 0.99, respectively. Note that the largest level of unbalance (m=2.7 grams) may have caused enough vibration at the damper to produce journal and bearing contact while passing

through the critical speed.

Analytical SFD coefficients have been estimated for the test damper configuration using the known damper geometrical parameters, a fluid viscosity of 0.00225 Pa-sec for an operating temperature of 29.5 C, and several damper orbit radius. Table 3 presents a summary of the results obtained from the formulae for the short SFD theory with the π film cavitation model. A comparison of the analytical direct damping coefficient C_{tt} with the experimentally based damping coefficients given in Table 2 shows good correlation only if the damper orbit radius is below 0.50. The measurements show that the analytical predictions of damping are excessively large for the largest unbalance tested.

TABLE 3. Estimated analytical SFD coefficients for circular centered motions at the natural frequency (34 Hz)

ε SFD orbit radius	C_{tt} (lb.s/in)	C_{rt} (lb.s/in)	K_{rr} (lb/in)
0.0	0.513	0.0	0.00
0.30	0.591	0.236	50.53
0.50	0.790	0.580	124.00
0.75	1.773	2.560	546.70
0.90	6.194	16.280	3478.00

Table 3 also shows values of the SFD radial stiffness coefficient at the system critical speed. This dynamic stiffness coefficient will act as an additional support in the system, modify its stiffness and rise the critical speed of the rotor-SFD apparatus. The value of the modified stiffness at the SFD location is then $K_{mod,SFD} = K_{SFD} + K_{rr} = 679.26$ lb/in + K_{rr} , and with an equivalent mass $M_{SFD} = 5.753$ lbs a modified system critical speed can be estimated. Table 4 shows the theoretical effects of the damper radial stiffness on the system stiffness and the predicted system critical speed as the SFD orbit increases. The experimental results for the unbalance response of the system, Figures 8 through 13, show a slight increase in the system critical speed as the disk unbalance increases. The experimental critical speed shift is not as pronounced as the analytical predictions estimate. On the other hand, if fluid inertia effects are accounted on the theoretical calculations, the system mass will also increase and determine lower values of the system critical speed. Recall that the estimated added mass of the SFD is equal to 0.344 kg (0.75 lb), and the modified critical speed for ε=0.75 would be 2,571 rpm..

TABLE 4. Effect of theoretical damper radial stiffness on system critical speed

ε SFD orbit radius	K_{rr} (lb/in)	$K_{mod,SFD}$ (lb/in)	ω_{crit} Hz	rpm
0.00	0.00	679.26	34	2,050
0.30	50.53	729.80	35.2	2,110
0.50	124.0	803.26	36.9	2,214
0.75	546.7	1,226.00	45.6	2,735

San Andres et al. (1988) presented an analysis for the unbalance response of rigid rotors and simple flexible rotors supported on short length, open ends SFDs. This study also includes fluid inertia effects for the case of centralized squeeze film dampers. Based on this study, Figure 20 presents the calculated synchronous forced response of the test apparatus for the different levels of disk unbalance tested. The system responses are shown at shaft location 1 using the conical model assumed. The predicted analytical response shows p-p amplitudes which correlate well with the measurements for disk unbalance masses equal to 1 and 2 grams (see Figures 8 and 9) . However, for the largest unbalance of 2.7 grams ($u_{SFD}/C=0.192$) the experimental curve does not show the broad response and bent typical of the analytical predictions around the resonance region. Furthermore, at this unbalance level the measurements show a much larger amplitude of motion than the calculations without a substantial shift in the critical speed. Figure 21 presents the frequency response including the effects of fluid inertia for the largest unbalance level ($u_{SFD}/C=0.192$). Note that fluid inertia reduces the non-linear effect and it also decreases even more the amplitude of motion at the critical speed. It is important to note that the rotor-SFD amplitudes of motion at the critical speed would have been significantly smaller (more damped) if a full film or uncavitated, short SFD model would have been used to evaluate the system frequency response.

Conclusions

The profusion of recent theoretical results addressing to the non-linear aspects of rotors mounted on SFDs has motivated the design, construction and testing of a small experimental apparatus for the measurement of the dynamic forced response of a rotor supported on open-ends SFDs with centering springs. The test apparatus consists of an overhung disk and shaft supported on a bronze bushing on the motor drive side and on ball-bearings with a squirrel cage elastic structure at the squeeze film damper location. The rig is fully instrumented with (X-Y) displacement probes at four locations along the shaft axis. In the tests reported the SFD journal was statically centered within its bearing and the level of external pressurization was kept low. Experimental measurements for coast-down tests with a controlled rotor deceleration rate were performed from 5,000 rpm and passing through the system first rigid body, conical mode critical speed at 2,000 rpm. The amplitude of rotor motion as a function of speed was recorded for three

levels of disk unbalance, and from these results experimental damping coefficients for the SFD were identified. A simple analytical model to describe the dynamics of the rotor-SFD system at rotational speeds below the first elastic critical speed has been proposed and theoretical damping coefficients estimated.

The experimental frequency response curves for disk unbalance excitation show the rotor-SFD to behave linearly with a well defined narrow critical speed region and large amplitudes of motion. An average experimental damping ratio approximately equal to 0.10 is obtained from the tests. Measurements of rotor amplitudes of motion at different shaft axial locations show the test apparatus to have a conical mode shape for speeds well below the first flexural mode. The experimental frequency responses due to unbalance excitation were purely synchronous in all the tests. The theoretical predictions, based on a simple equivalent mechanical model for conical motion, show the rotor-SFD test rig to have a characteristics nonlinear frequency response for the largest level of unbalance with a shift in the critical speed and with a broader speed region where amplitudes of motion are significant. The measured amplitudes of motion at the shaft free end are substantially larger than the analytical predictions, and these also determine smaller damping coefficients at the SFD location. Further tests with larger levels of disk unbalance were not performed to protect the test apparatus, although the maximum unbalance level used appears to be small from a theoretical point of view.

Experimentally identified direct damping coefficients correlate well with theoretical values based on small to moderate journal orbit radii, but are far too small when compared with the values calculated from the analytical formulae using the measured orbit radii. Predicted SFD radial stiffnesses are too large, and if present, their effect was not ever observed on the frequency response measurements. The measurements then prove that the response of the rotor-SFD apparatus can be described accurately by a linear model for the damper element rather than by the complex non-linear SFD formulation based on traditional lubrication approaches.

Further tests for measurement of the rotor-SFD rig unbalance response with the journal statically off-centered are planned for the Summer'94. A current proposal to NSF on this same subject has very good possibilities of being funded. The experimental program will concentrate on the design and construction of a better and more realistic rotor-SFD apparatus for controlled dynamic tests if the NSF project is awarded.

REFERENCES

(1) Wort, J.F.G., "Fundamentals of Balancing Machines," B&K Technical Review, 1 (1981).

(2) Myklestad, N.O., "A New Method of Calculating Natural Modes of Uncoupled Bending Vibration of Airplane Wings and other types of Beams," Journal of the Aeronautical Sciences, pp. 153-162 (April 1944).

(3) Prohl, M.A., "A General Method for Calculating Critical Speeds of Flexible Rotors," Journal of Applied Mechanics, pp. A-142-A-148 (September 1945).

(4) Vance, J.M., Murphy, B.T., and Tripp, H.A., "Critical speeds of Turbomachinery: Computer Predictions vs. Experimental Measurements," Proceedings of the Thirteenth Turbomachinery Symposium, Texas A&M University, November 13-15, 1984, p. 105-130.

(5) Childs, D., 1993, "Turbomachinery Rotordynamics," Wiley Interscience Publishing Co.

(6) Vance, J.M., 1988, "Rotordynamics of Turbomachinery," Wiley Interscience Publishing Co.

(7) San Andres, L.A. and Vance J.M., 1988, "Effects of Fluid Inertia on the Performance of Squeeze Film Damper Supported Rotors," ASME Journal of Engineering for Gas Turbines and Power, Vol. 110, pp. 51-57.

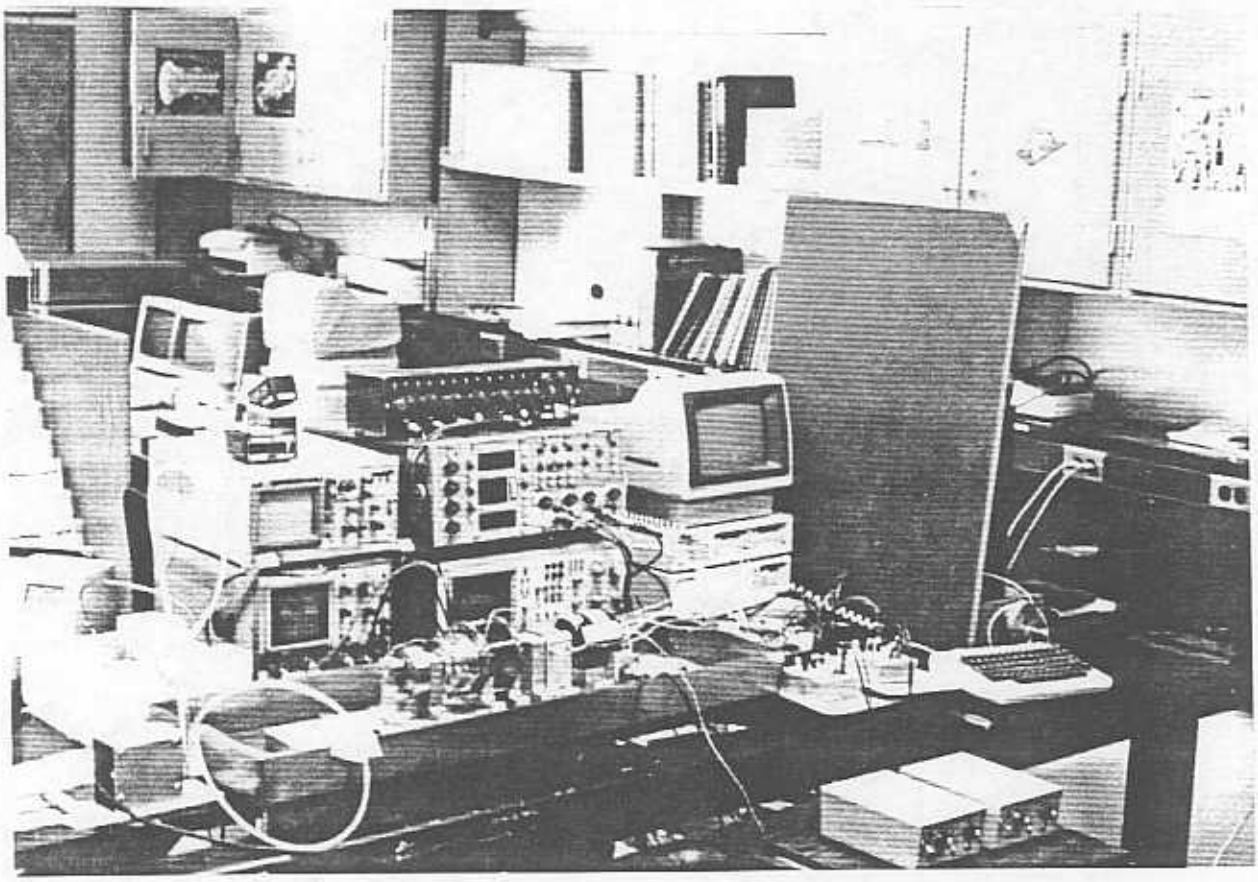

Figure 1 Picture of the test-rig apparatus and Instrumentation

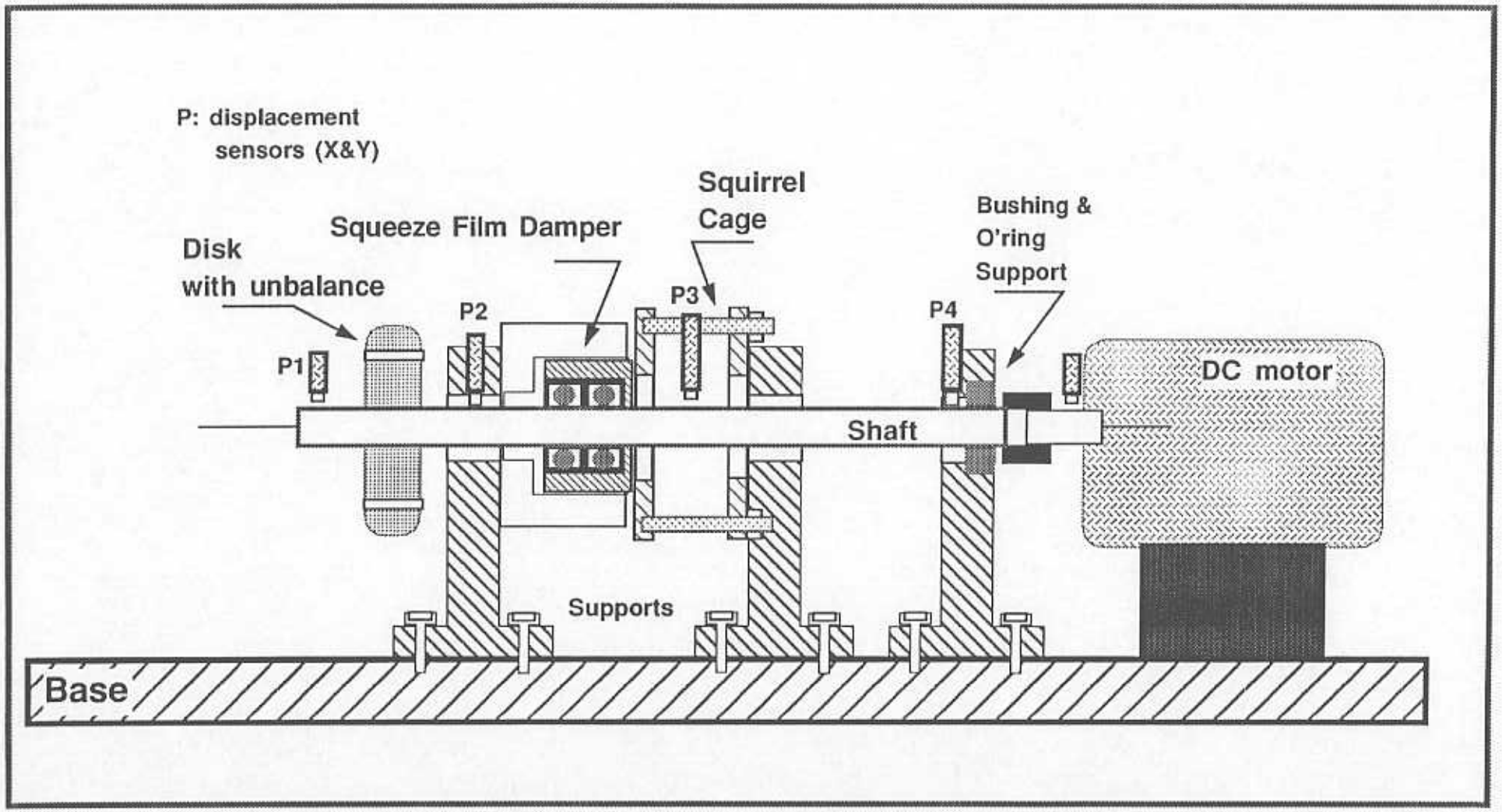

Figure 2. Rotor – Squeeze Film Damper Test Apparatus

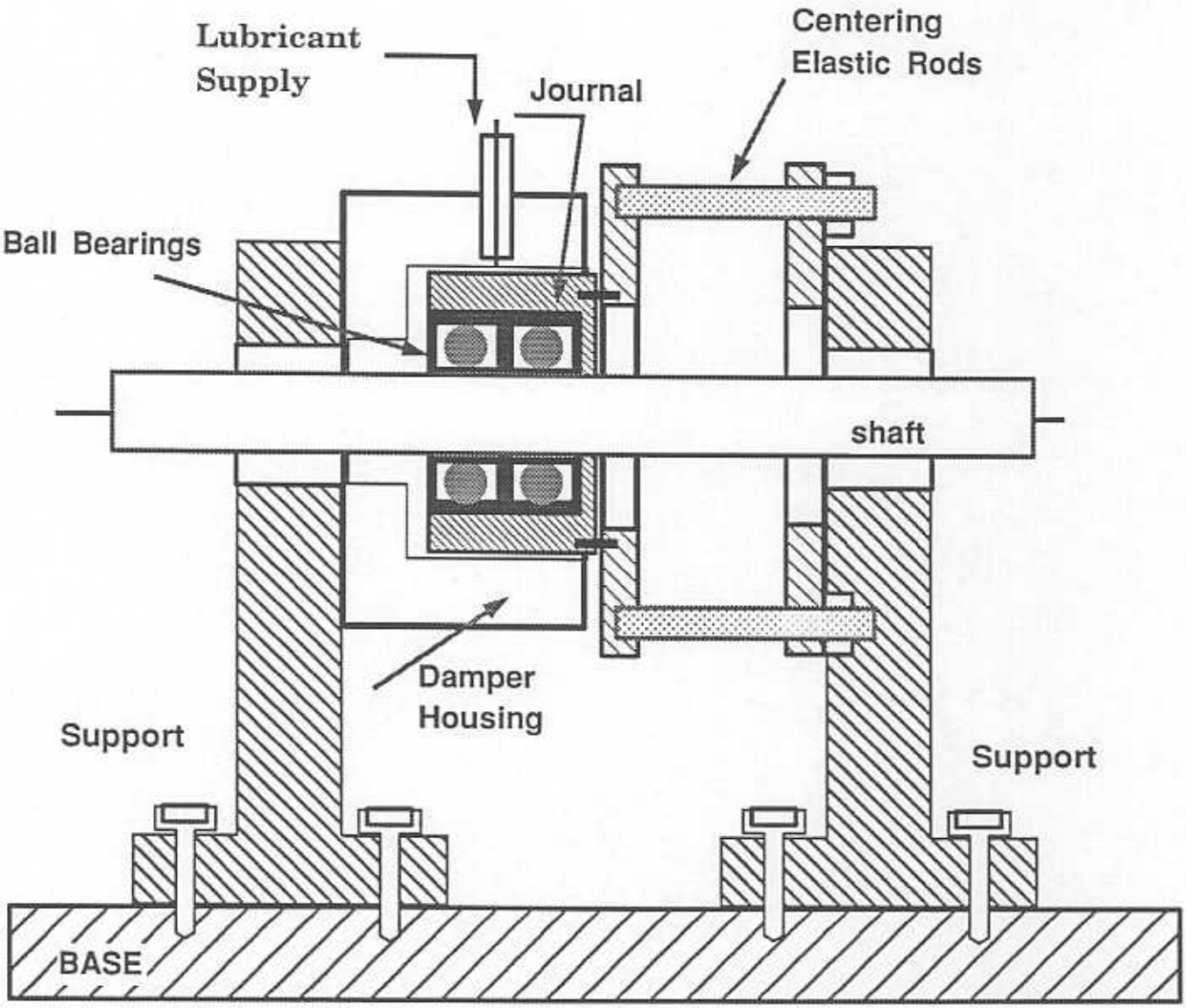

Figure 3. Squeeze Film Damper and Squirrel Cage Assembly.

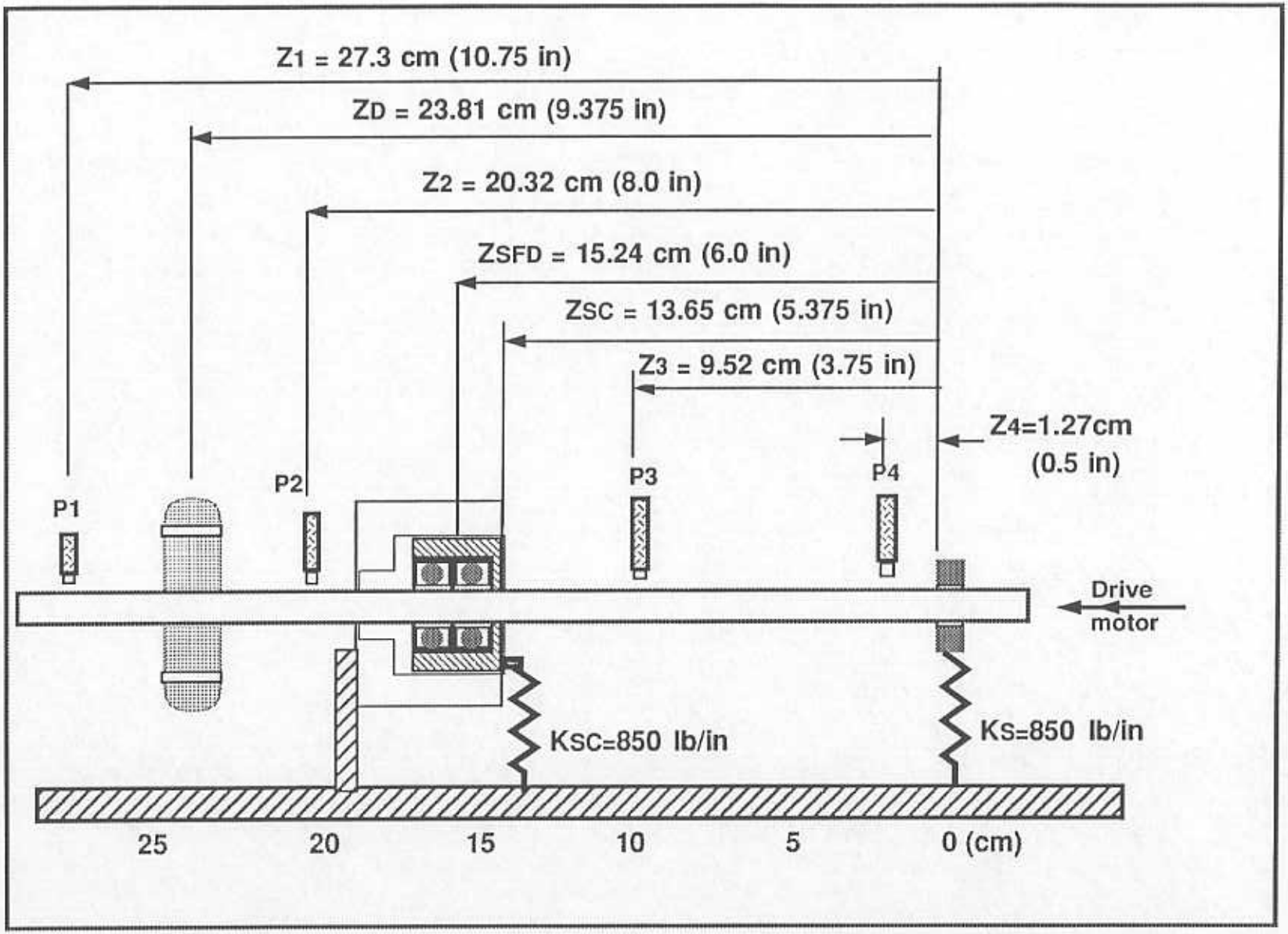

Figure 4. Rotor–SFD test rig: Location of displacement sensors and dimensions.

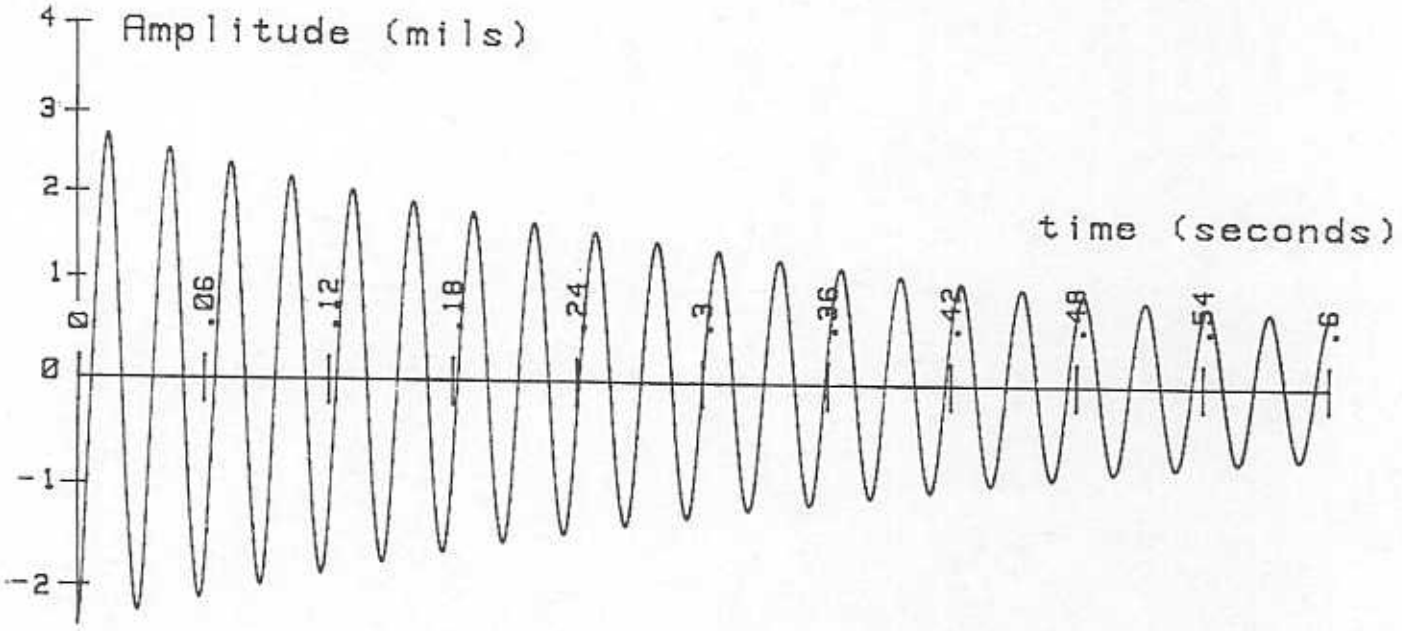

Figure 6 Free vibration test at location P1 without oil in the damper . Rotor speed zero rpm
ω_n = 34.1 Hz, ξ = 0.0099, logdec= 0.0622

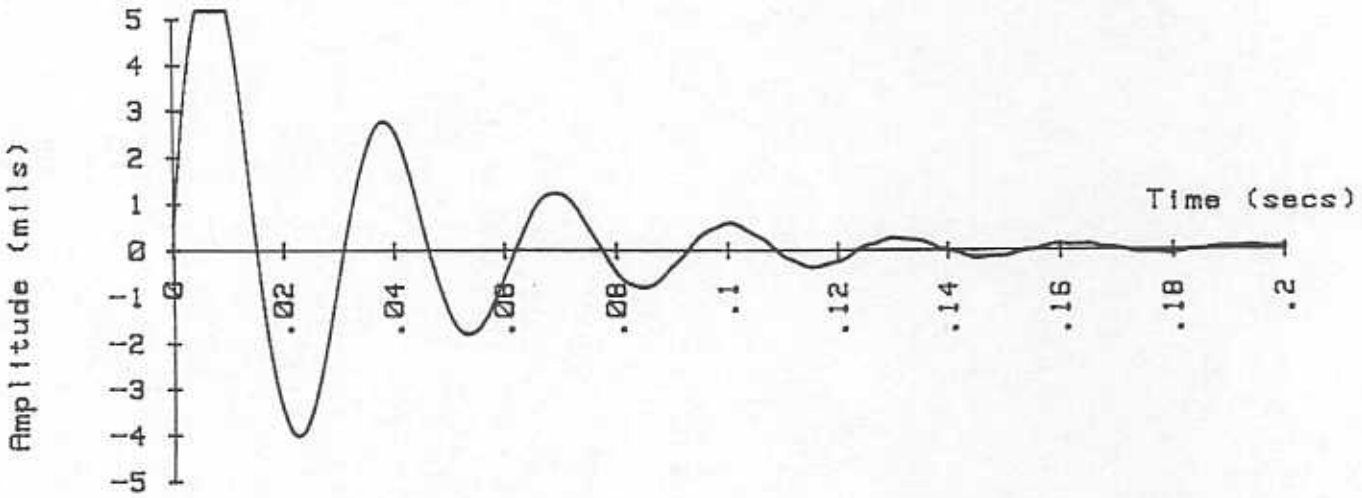

Figure 7 Free vibration test at location P1 with oil in the damper . Rotor speed zero rpm
ω_n = 32.0 Hz, ξ = 0.124, logdec= 0.779

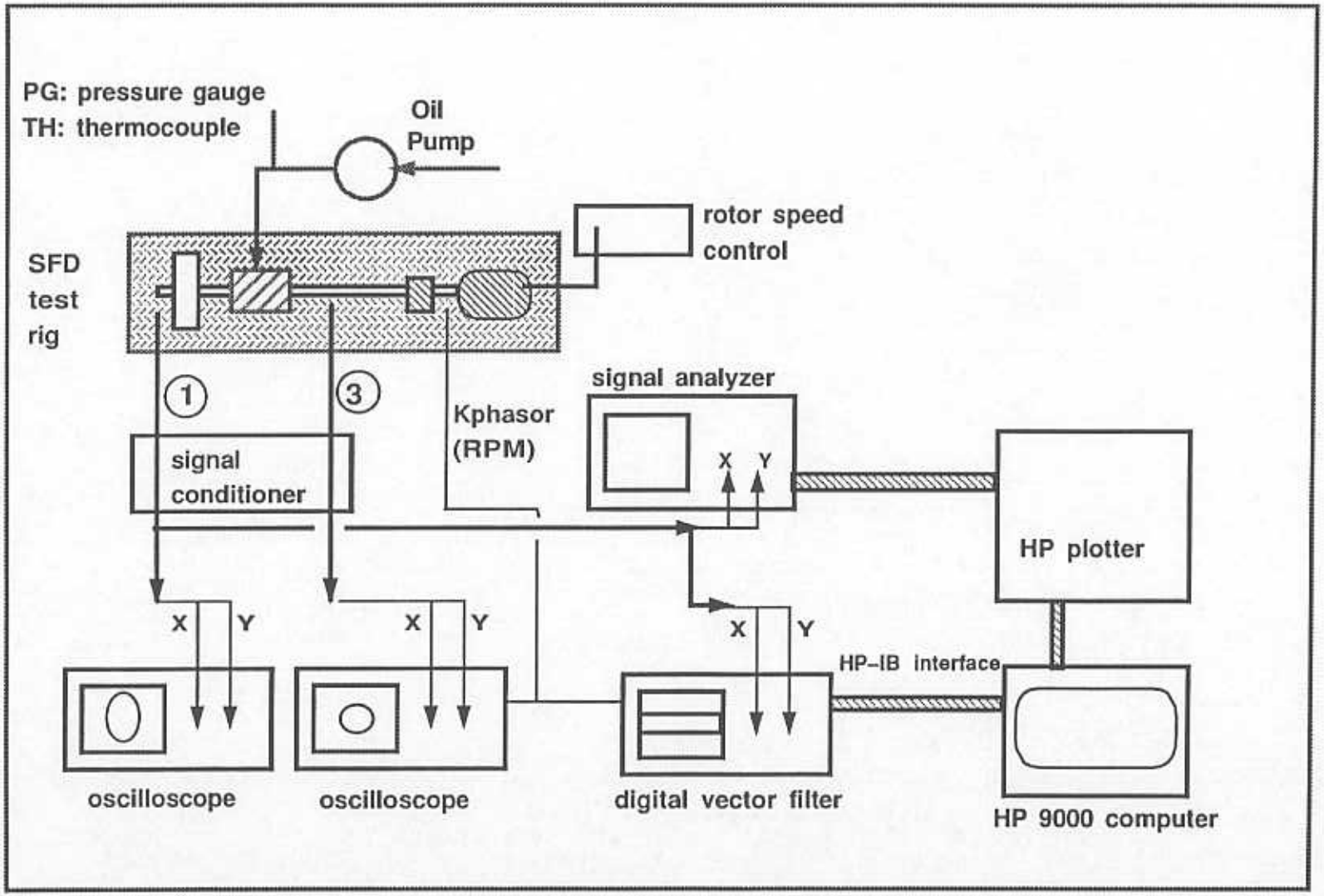

Figure 5. Schematic view of instrumentation for rotor–SFD test rig.

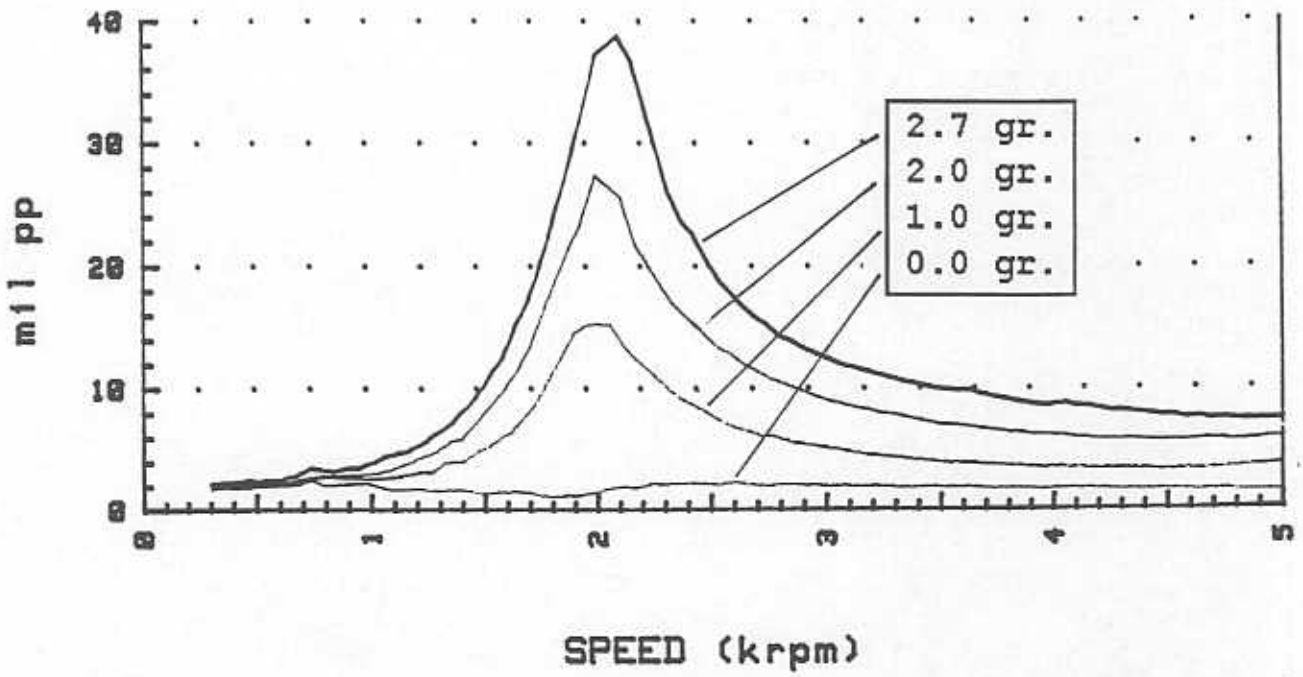

Figure 8 Rotor unbalance response at location P1 (vertical direction), for disk unbalance masses of 0, 1.0, 2.0 and 2.7 gr.

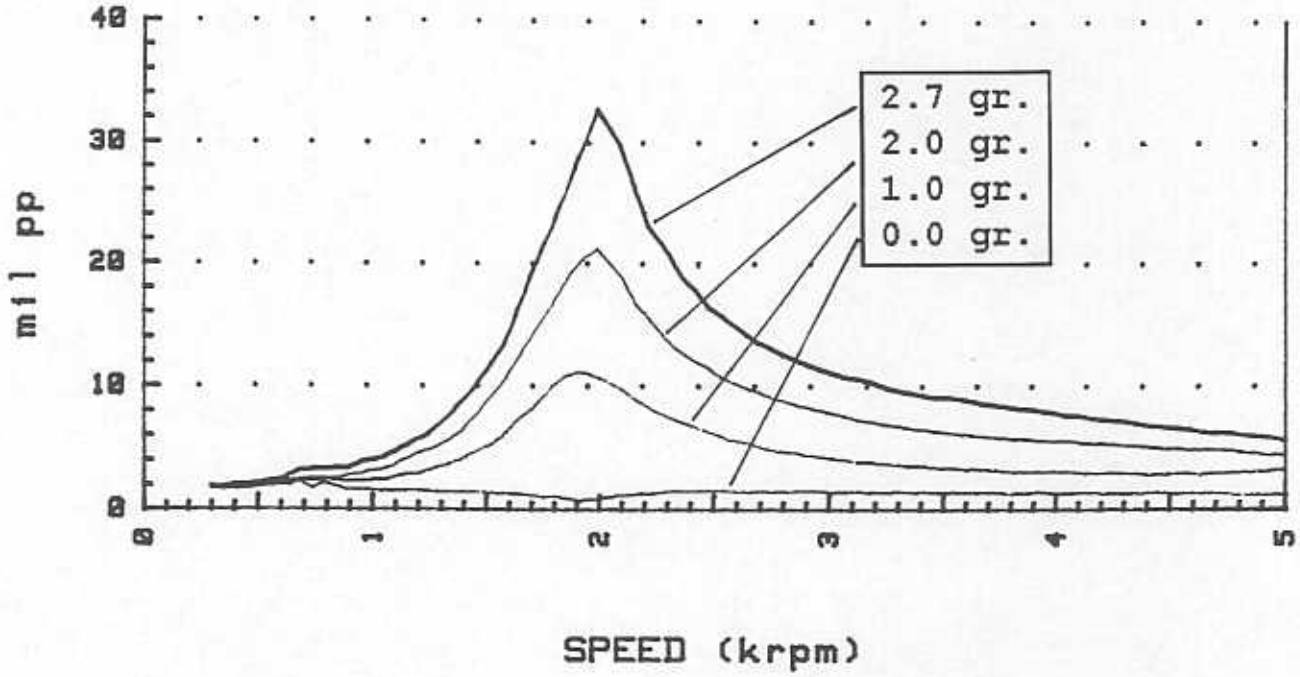

Figure 9 Rotor unbalance response at location P1 (horizontal direction), for disk unbalance masses of 0, 1.0, 2.0 and 2.7 gr.

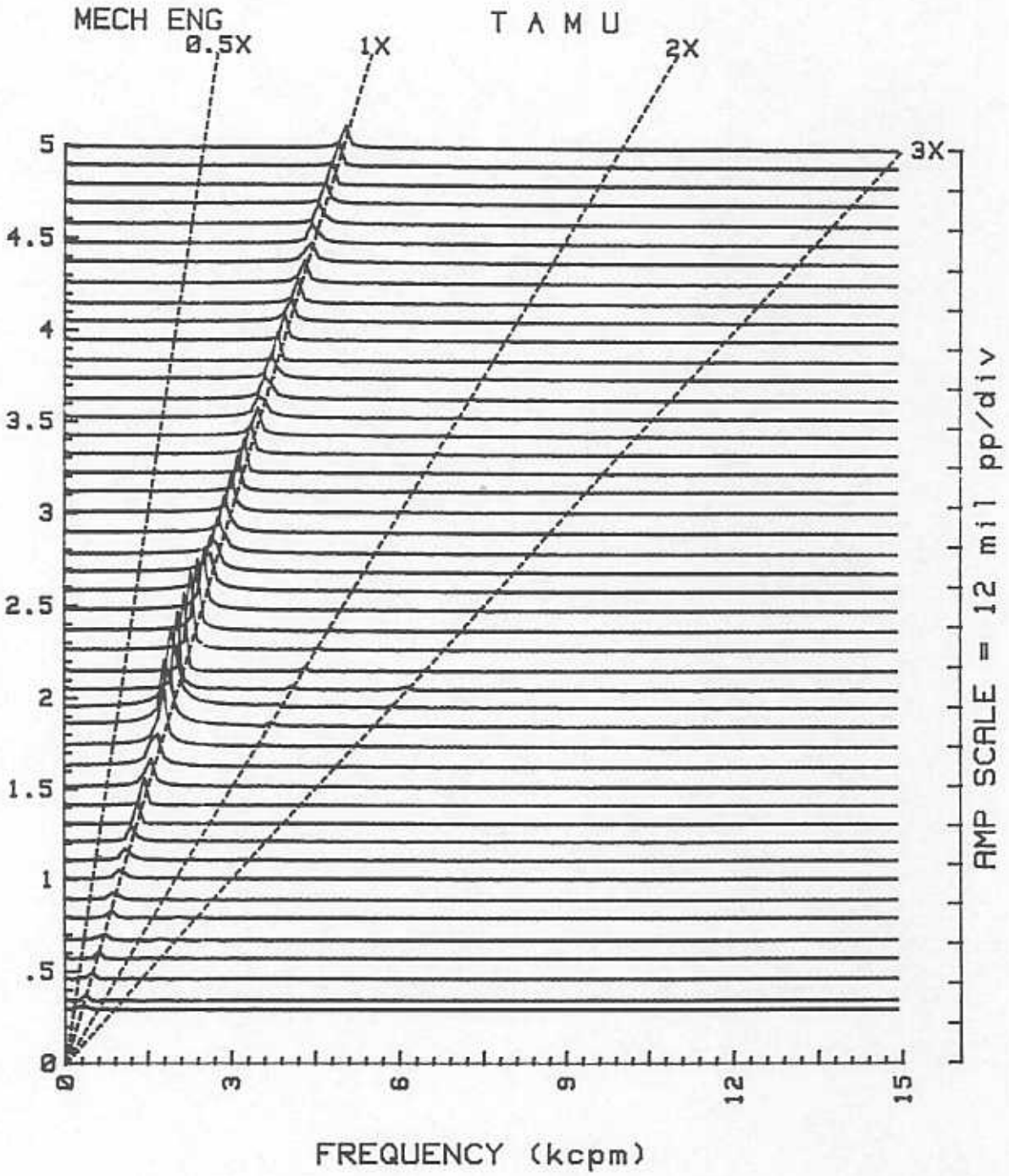

Figure 10 Cascade Plot at rotor position P1
(vertical direction)
for disk unbalance mass 2.7 gr.

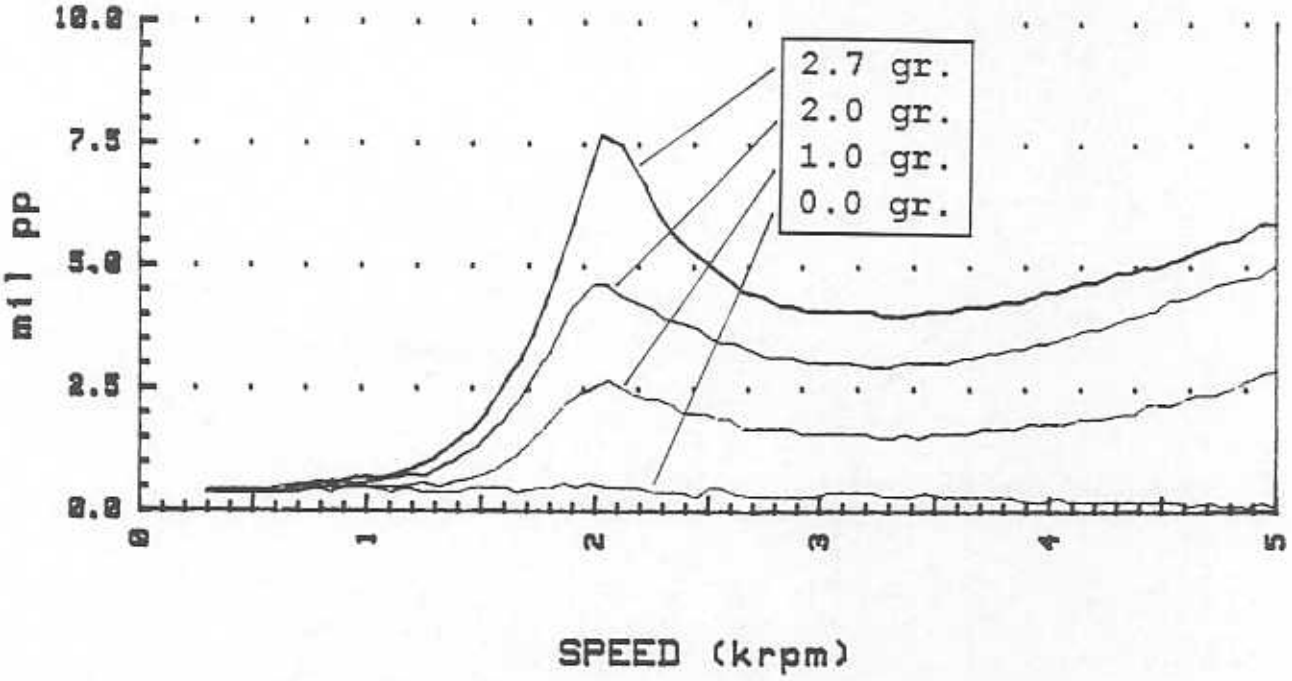

Figure 11 Rotor unbalance response at location P3 (vertical direction), for disk unbalance masses of 0, 1.0, 2.0 and 2.7 gr.

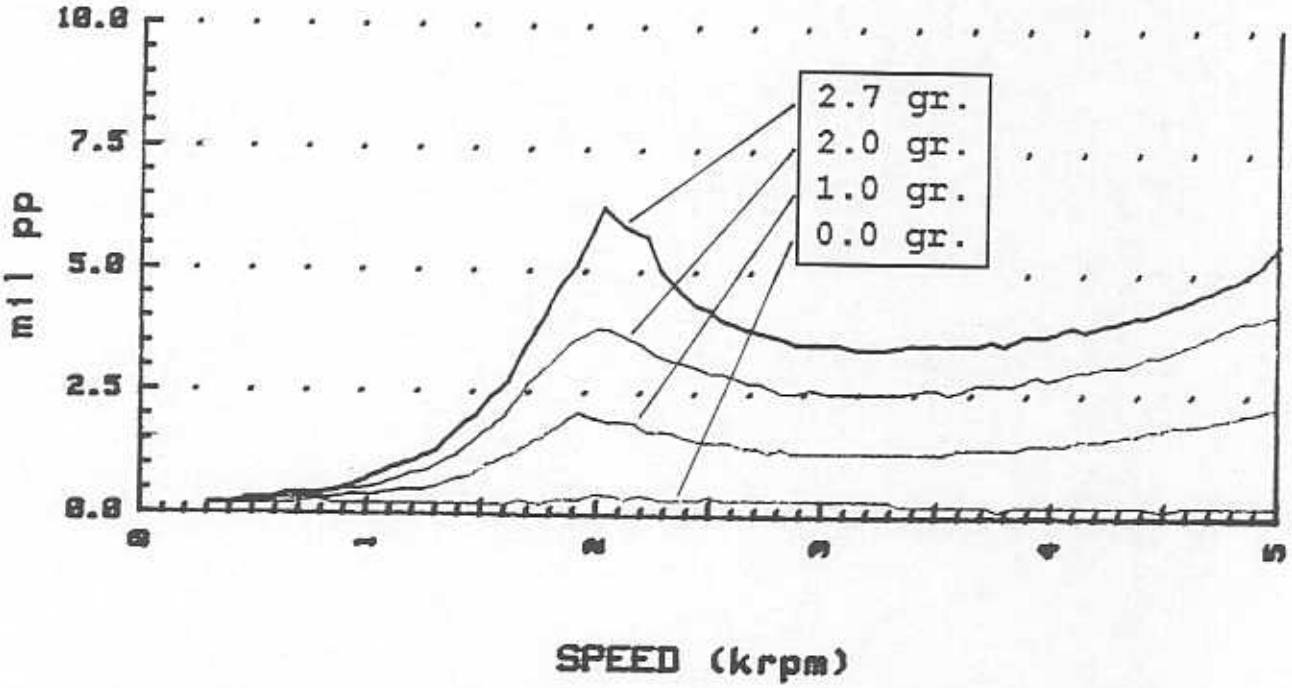

Figure 12 Rotor unbalance response at location P3 (horizontal direction), for disk unbalance masses of 0, 1.0, 2.0 and 2.7 gr.

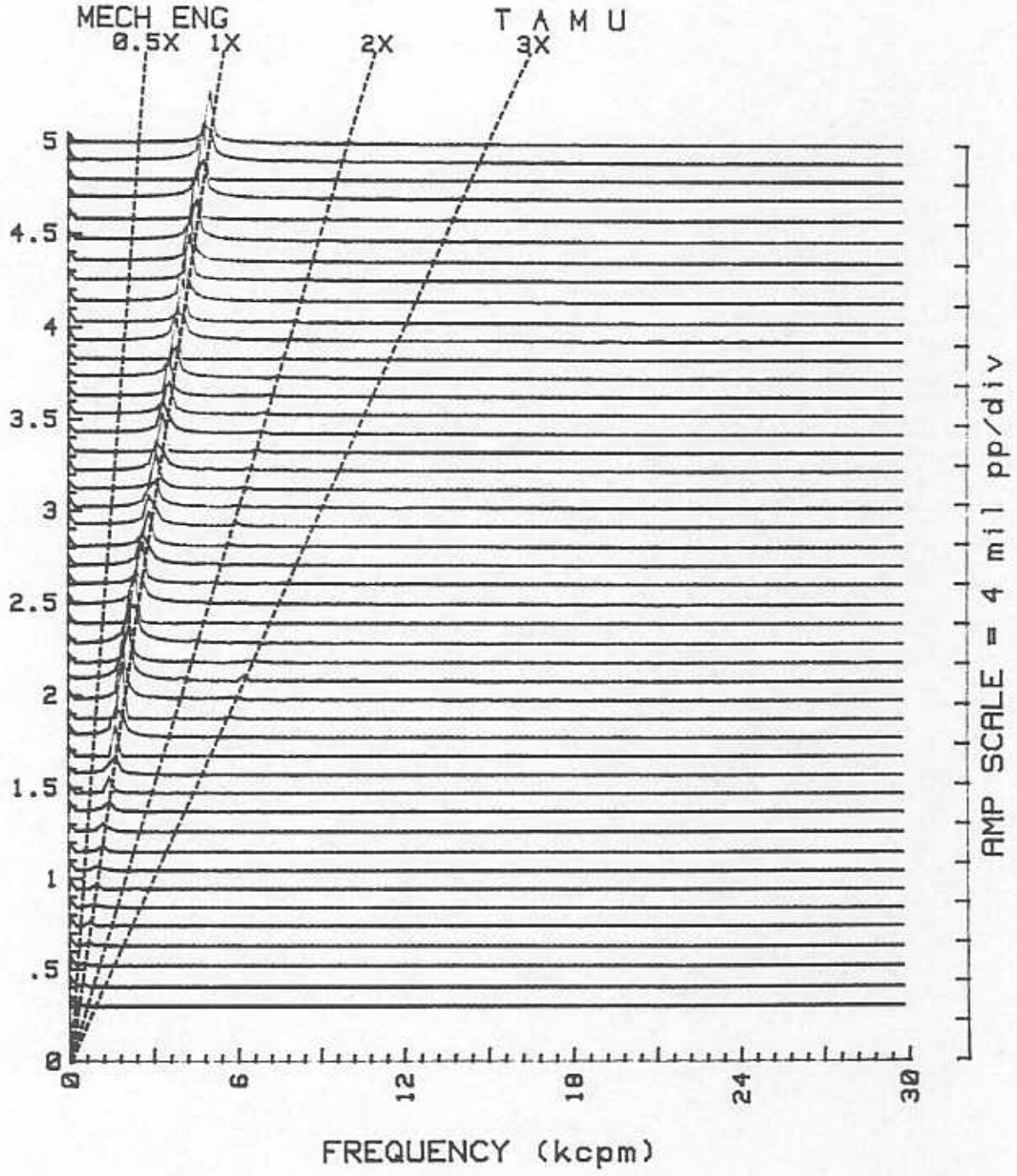

Figure 13 Cascade Plot at rotor position P3
(vertical direction)
for disk unbalance mass 2.7 gr.

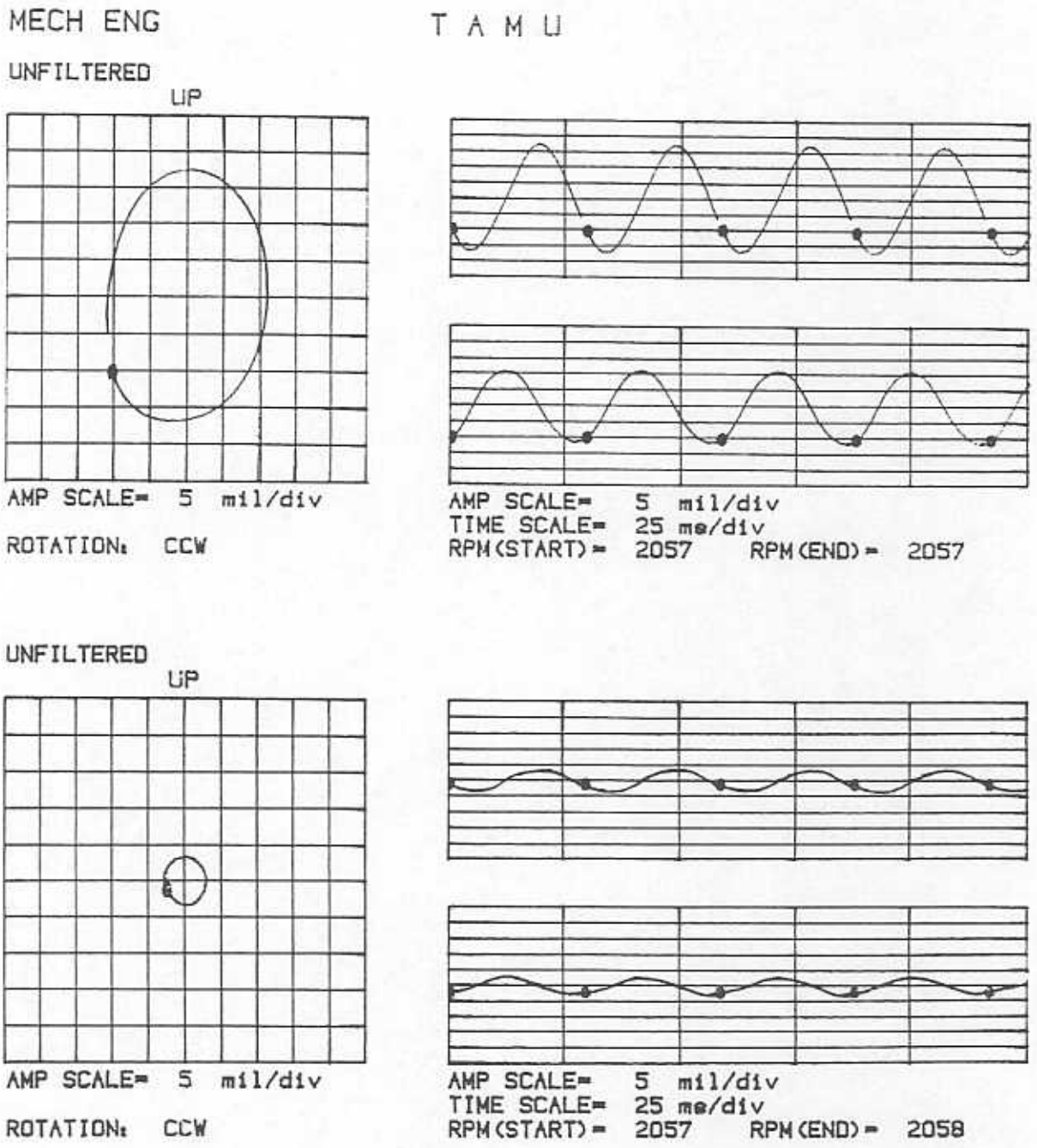

Figure 14 Orbit Plots at rotor positions P1 and P3 at 2057 rpm, disk unbalance mass 2.7 gr.

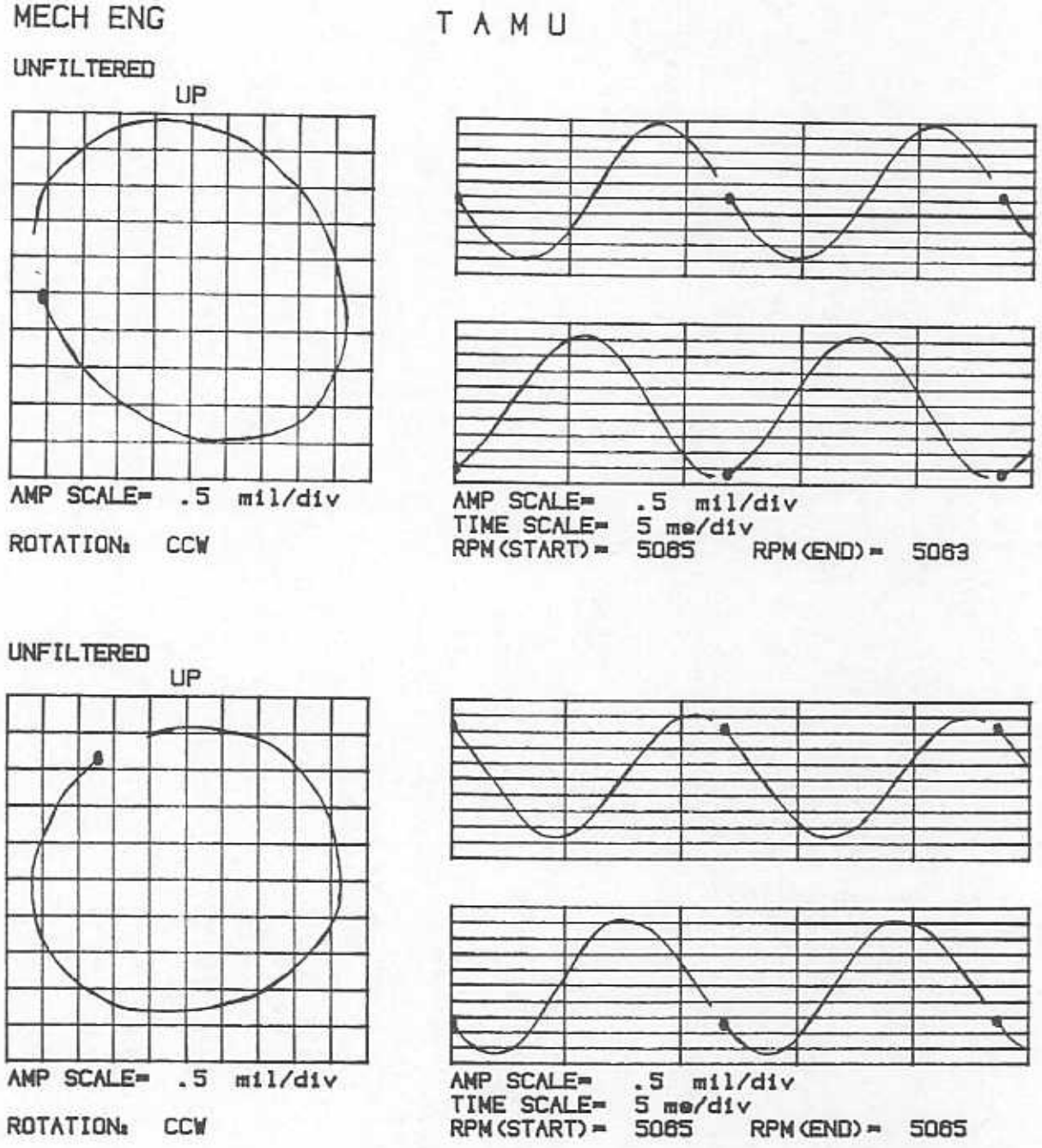

Figure 15 Orbit Plots at rotor positions P1 and P3 at 5065 rpm, disk unbalance mass 2.7 gr.

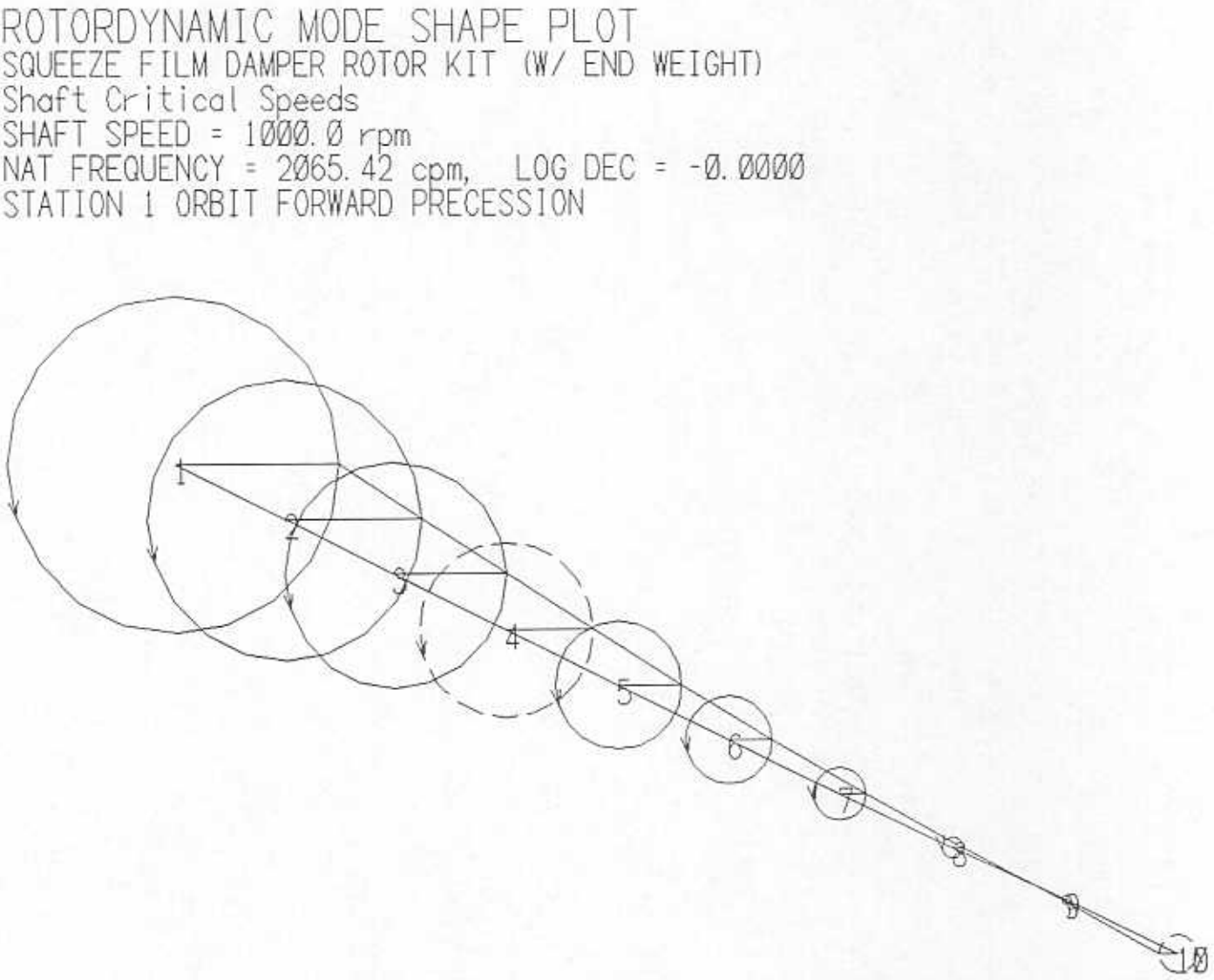

Figure 16 Predicted undamped first mode shape for rotor-SFD apparatus.
ω_{n1} = 34.4 Hz
Disk at station 1
SFD at station 4
Support at station 10

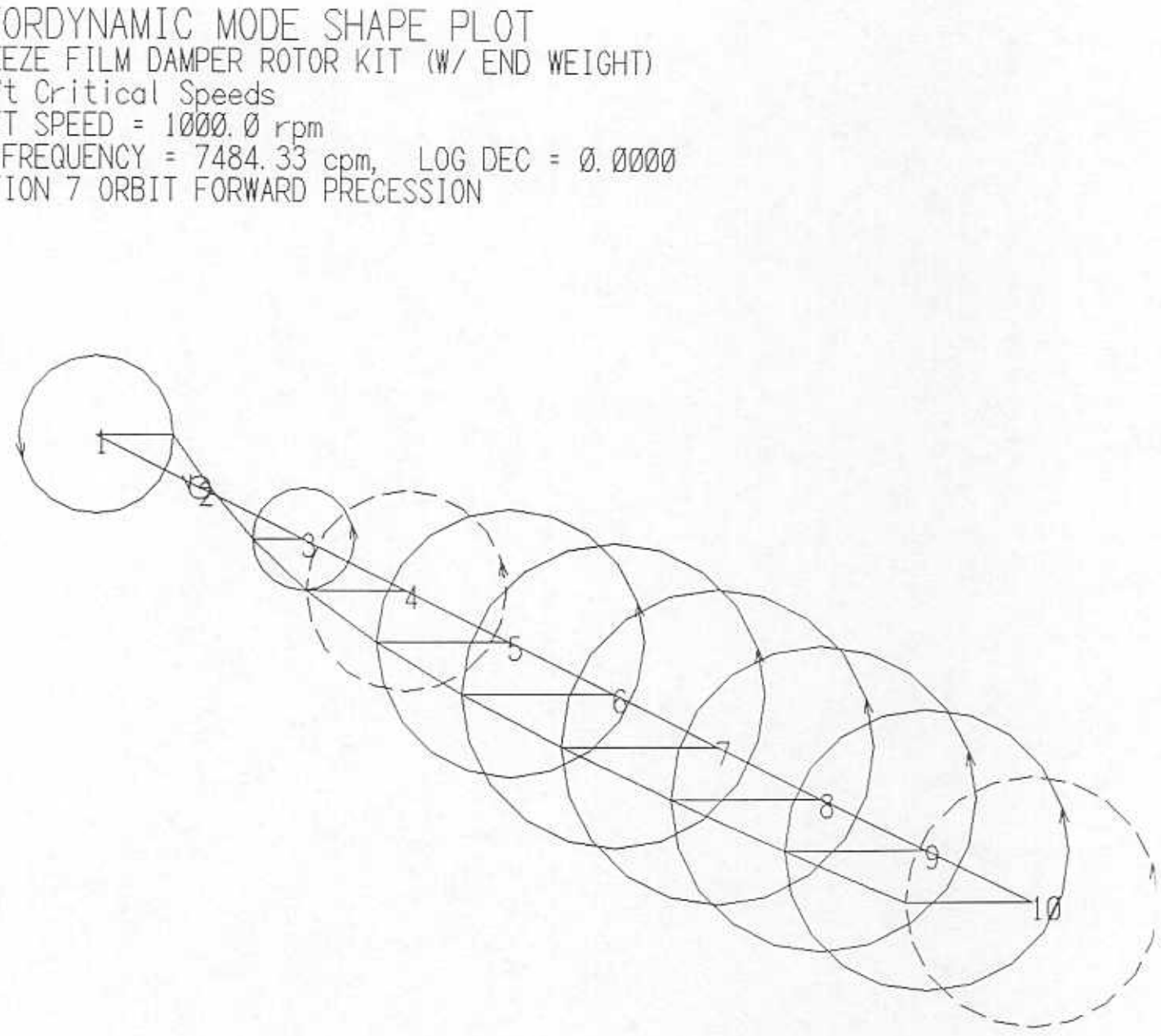

Figure 17 Predicted undamped second mode shape
for rotor-SFD apparatus.
ω_{n2} = 124.7 Hz
Disk at station 1
SFD at station 4
Support at station 10

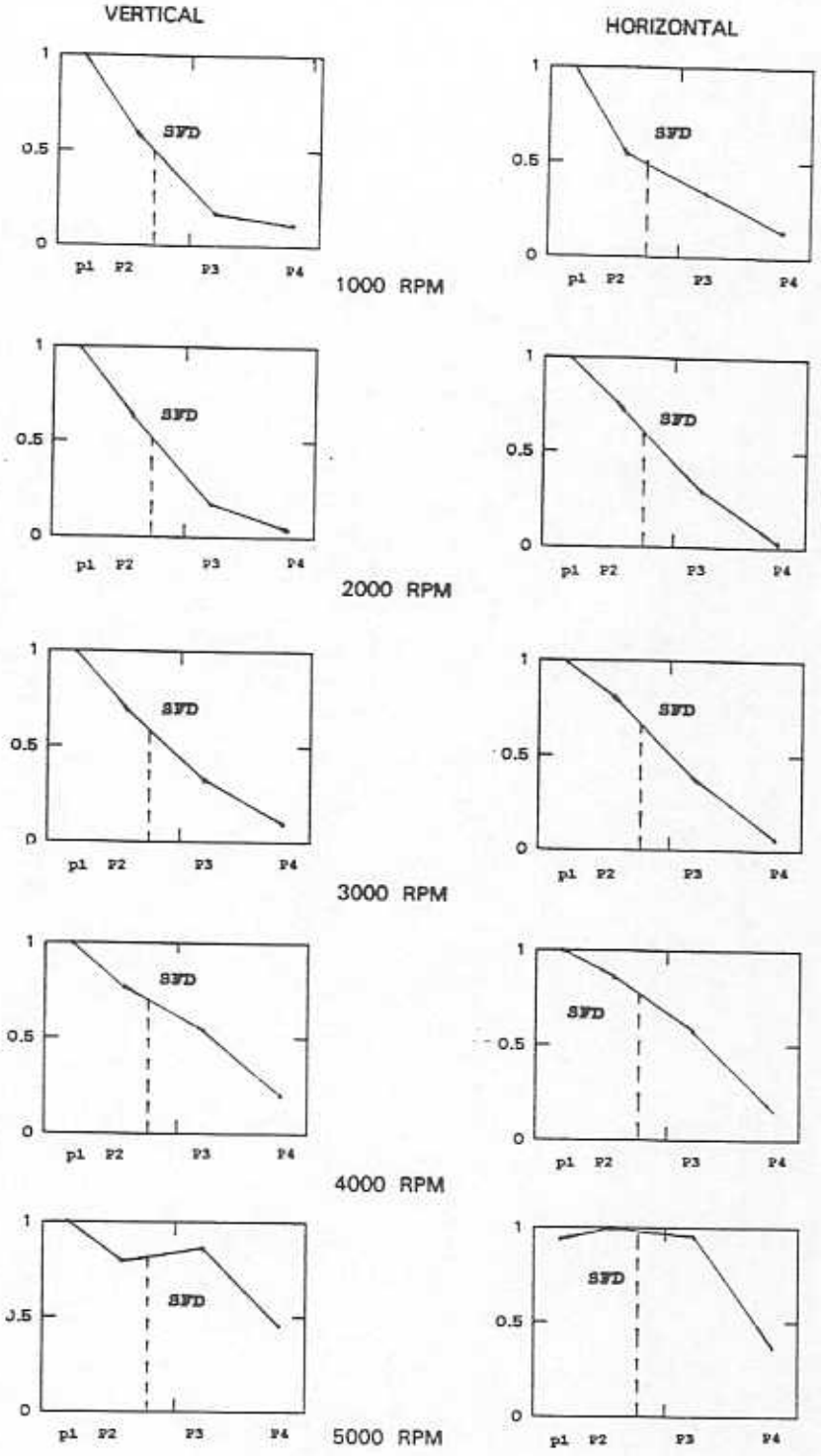

Figure 18 Measured vibration shapes at shaft locations 1 to 4 for rotor-SFD apparatus as shaft speed increases

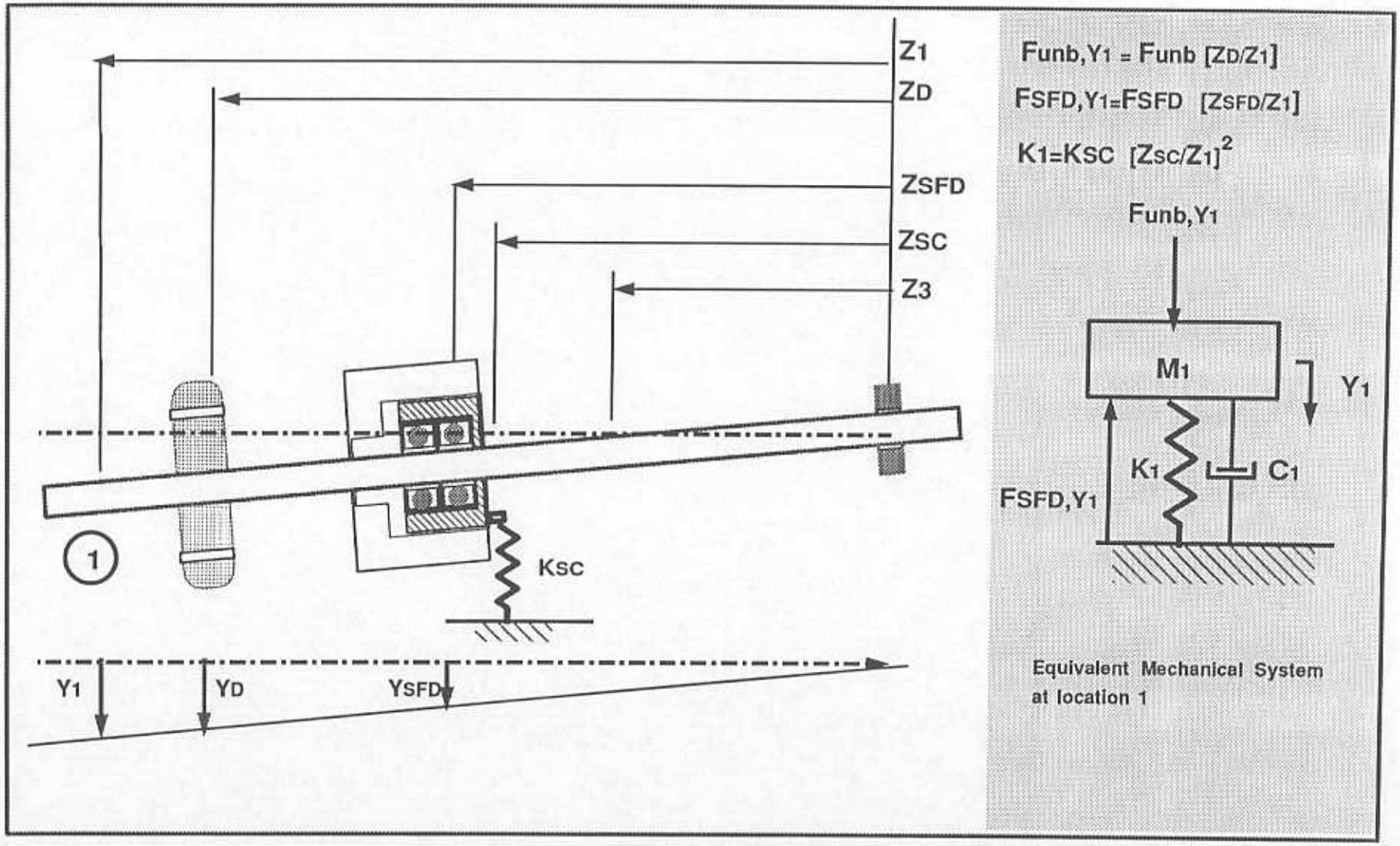

Figure 19. Assumed conical mode shape for SFD–rotor rig and equivalent mechanical system at location 1.

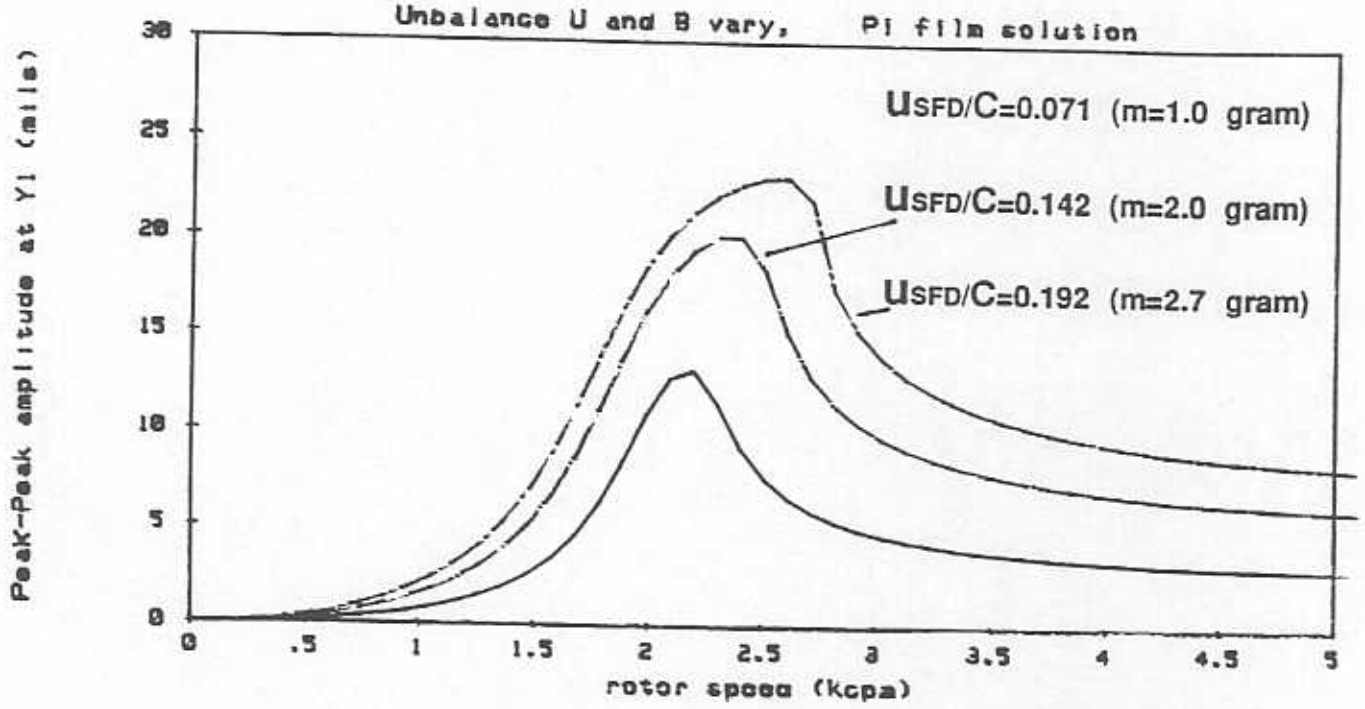

Figure 20. Theoretical dynamic forced response of rotor–SFD test rig at Y1. Short length, open ends π film SFD. No fluid inertia Unbalances U_{SFD}/C=0.071, 0.142, 0.192 (m=1, 2, 2.7 grams).

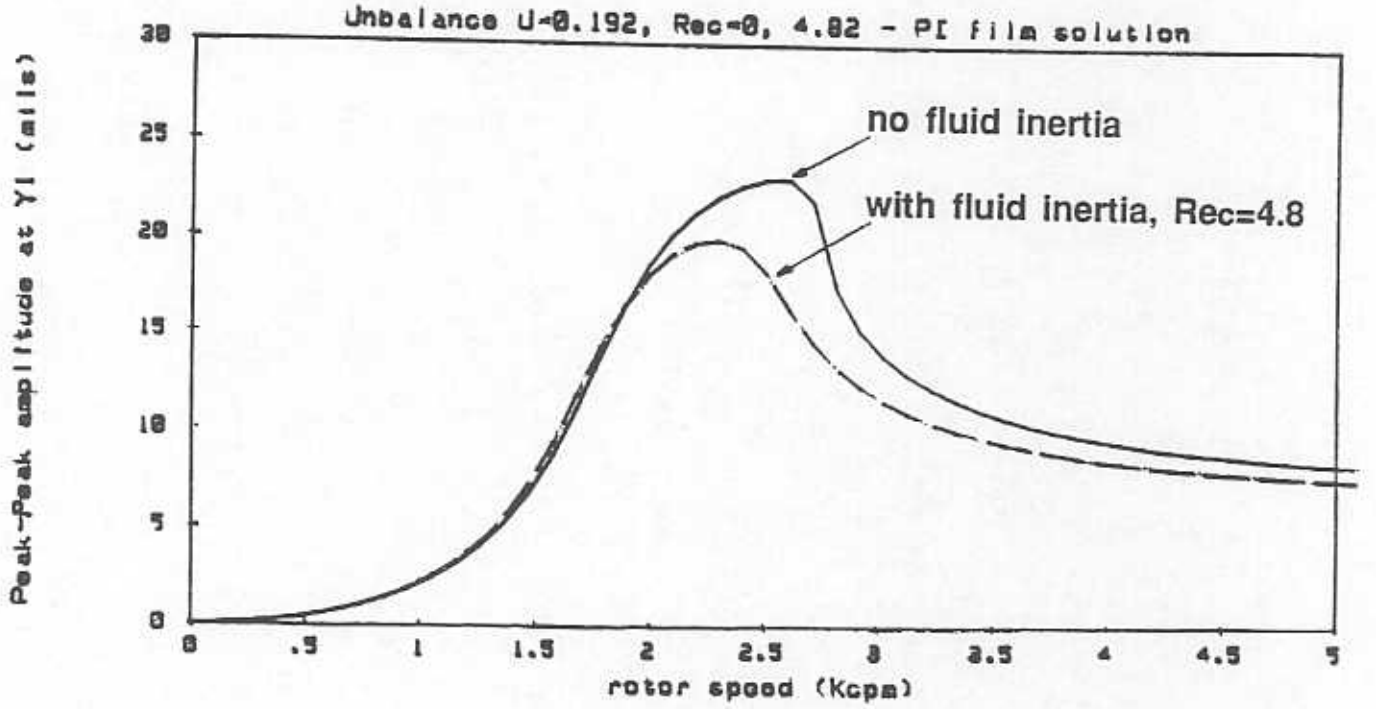

Figure 21. Effect of fluid inertia on the theoretical dynamic fored response of rotor–SFD test rig at Y1. Short length, open ends π film SFD. Unbalance U_{SFD}/C=0.192 (m=2.7 grams).